ENHANCING THE AERODYNAMIC PERFORMANCE

OF

STEPPED AIRFOILS

by

RANGANADHAN VOONA

A THESIS

Presented to the Graduate Faculty of the

MISSOURI UNIVERSITY OF SCIENCE AND TECHNOLOGY

In Partial Fulfillment of the Requirements for the Degree

MASTER OF SCIENCE IN MECHANICAL ENGINEERING

2012

Approved by

Fathi Finaish, Advisor
K. M. Isaac
Serhat Hosder

ABSTRACT

The main objective of this research was to investigate the lift and drag characteristics of a stepped airfoil with backward facing steps; apply active flow control technique to enhance the aerodynamic performance of stepped airfoils and examine the possibility of using such airfoils on Unmanned Aerial Vehicles (UAV's). A step was introduced at mid-chord, with a depth of 50% of the airfoil thickness at mid-chord position extending till the trailing edge of a NACA 4415 airfoil. Computational studies were conducted with the use of passive flow control constituting the activation of step and active flow control with the use of air injecting jets placed in the step cavity of the NACA 4415 airfoil with a goal of enhancing the aerodynamic performance. The jet angle and jet momentum coefficient were varied independently to identify the best setting for optimizing the aerodynamic performance of the stepped airfoil. Experimental studies of a scaled wing model with the same airfoil were conducted in a wind tunnel for a range of Reynolds numbers to validate some of the numerical results obtained for the cases of base and stepped airfoils. The results produced show that as much as 37% increase in C_l and as much as 12 % increase in L/D ratios over conventional airfoil values could be obtained using stepped airfoils and further enhancement could be made with the employment of jets placed in the step cavities.

The case study conducted as a part of this research focuses on the UAV RQ-2 Pioneer employing a stepped airfoil configuration by comparing its aerodynamic characteristics with the conventional NACA 4415 airfoil originally used on this aircraft. The primary objective of the case study was to identify and outline a step schedule for the flight envelope of the UAV Pioneer using a stepped airfoil configuration while applying active flow control to obtain enhanced aerodynamic performance over conventional NACA 4415 airfoil originally used and hence improve the flight performance characteristics like Range and Endurance of the aircraft.

ACKNOWLEDGMENTS

I would like to thank Dr. Fathi Finaish for his guidance, support and motivation throughout the period of my research under his stewardship. I extend my sincere thanks to the Department of Mechanical and Aerospace Engineering for funding me through their Teaching Assistantship and Departmental Fellowship programs.

I wish to acknowledge the distinguished members of my thesis committee for valuable pieces of advice which helped me draft a well-structured thesis. I extend my sincere thanks to James Schneider of the Aerospace Flow Laboratory who was extremely helpful in setting up the experimental apparatus and offered his full support through the length of my experimental work at Missouri S&T. I also wish to thank Mariana Escalona Diaz who showed interest in subject discussions pertaining to her undergraduate research at Missouri S & T.

My mother without whose support and faith in me my research would not have been possible deserves a worthy mention here.

TABLE OF CONTENTS

LIST OF ILLUSTRATIONS

Figure Page

LIST OF TABLES

NOMENCLATURE

Symbol	Description
c	airfoil chord
S	wing area
t	airfoil thickness at step leading edge
x	distance from leading edge
x_u	distance from airfoil LE to upper surface step LE
x_l	distance from airfoil LE to lower surface step LE
X_u	dimensionless upper surface step location, x_u/c
X_l	dimensionless lower surface step location, x_l/c
l_u	length of upper surface step
l_l	length of lower surface step
d_u	depth of upper surface step
d_l	depth of lower surface step
L_u	dimensionless upper surface step length, $1_u/c$
L_l	dimensionless lower surface step length, l_l/c
D_u	dimensionless upper surface step depth, d_u/t
D_l	dimensionless lower surface step depth, d_l/t
U_∞	free stream velocity
P	local pressure on airfoil surface
P_∞	free stream pressure
ρ_∞	free stream density
μ	dynamic viscosity of air
Re	Reynolds number, $\rho U_\infty c/\mu$
α	angle of attack

q_∞	free stream dynamic pressure, $1/2\rho U^2_\infty$
C_d	drag coefficient, $D/q_\infty S$
C_l	lift coefficient, $L/q_\infty S$
C_p	pressure coefficient, $(P - P_\infty)/q_\infty$
D	drag
L	lift
T	engine thrust available
V	velocity magnitude
v	dimensionless velocity
X	direction along the axis X
Y	direction along the axis Y
V_j	velocity of the jet
m_j	mass flow rate of the jet
ζ	jet angle
C_μ	jet momentum coefficient
g	acceleration due to gravity
S_{TO}	take-off distance
W_0	maximum weight of the aircraft RQ-2 Pioneer
W_1	empty weight of the aircraft RQ-2 Pioneer
μ_r	rolling friction coefficient
C_{lmax}	maximum value of the lift coefficient
E	endurance
η	highest propeller efficiency
c_s	lowest specific fuel consumption of the piston engine used on RQ-2 Pioneer

1. INTRODUCTION

Since the advent of successful aviation in commercial, defense and experimental research sectors, people have been constantly researching on improving the quality of flow over the aircraft so as to enhance the overall performance in terms of lift, drag and stability characteristics. Flow control has been and still is one of the most promising areas in aerodynamic research and will continue to be a prospective research topic as there will always be an upper limit to efficiency. Flow over submerged bodies such as an aircraft[22] and or a submarine can be worked upon to delay boundary layer transition, postpone separation, increase lift, reduce skin-friction and pressure drag, augment turbulence, enhance heat transfer, or suppress noise. Preventing separation is highly critical as it is desirable for lift enhancement, stall delay, improved pressure recovery, and reduction in the form drag. Future applications in the field of aeronautics include providing structurally efficient alternatives to flaps or slats; cruise application on conventional takeoff and landing aircraft including boundary layer control on thick span-loader wings; as well as increased leading edge thrust, and enhanced fuselage and upper surface lift with most of the new developments to be made pertain to the employment of various flow control techniques. Thus far, extensive research was done in passive flow control that involves control of flow sans use of external energy. Active flow which involves energy expenditure has been a hot topic of research in the recent decades and promises to be good for the future developments to come in the area of flow control. This research focuses on using both these techniques to enhance the aerodynamic performance of airfoils.

A promising passive flow control technique which is primarily dealt with in this study might be to modify the geometry of a conventional airfoil by introducing backward facing steps, which forms a relatively new family of airfoil designs popularly known as “KF (Kline-Fogleman) airfoils”. Introduction of a step could be greatly effective in changing the overall flow quality in

the step cavity, which may not be quite obvious to intuition. The flow transformation could be understood as due to rotation of the flow promoted by the introduction of the step along a length of an airfoil edge which otherwise had been continuous. Stepped airfoils use the concept of trapped vortex cavities and consequently there is the trapped vortex flow control which deals with the various flow alteration techniques to enhance the flow field characteristics. The flow which otherwise had been separated is forced to reattach by an intense system of vortices trapped in the cavity. Figure 1-1 compares the flow over a conventional with that over a modified airfoil with a step. Flow rotation induced near the step face generates a primary vortex as shown in Figure 1-2. A secondary vortex forms in the opposite direction after the flow reattaches itself to the boundary. Thus an airfoil with a step traps vortices in the cavity which primarily are the noticeable as well as distinguishing flow features as compared with the flow over conventional airfoils. The formation of these vortices alter the flow field characteristics thereby altering the lift, drag or pitching moment characteristics depending on whether the step is introduced on the upper or lower edge of the airfoil. The advantage of using the passive flow control technique of trapped vortex cavities is that the existence of the cavity on an airfoil / wing surface naturally aids the formation of vortices inducing reattachment of flow thus requiring no additional energy expenditure. An intelligently engineered design of the cavity could very well help get the best out of the flow field thereby eliminating the need for use of energy to achieve the desired flow quality.

In addition to passive flow control techniques, active flow control could possibly be used for obtaining positive results. Active flow control involves usage of energy to alter the flow field characteristics, meaning the use of either blowing or suction to control the flow near the boundary as to prevent flow separation. Flow control through blowing could be accomplished using air injecting jets or plasma actuators mainly to generate a directed stream of fluid to accelerate the slow moving air near the solid boundary thus delaying separation. Also, suction created using a

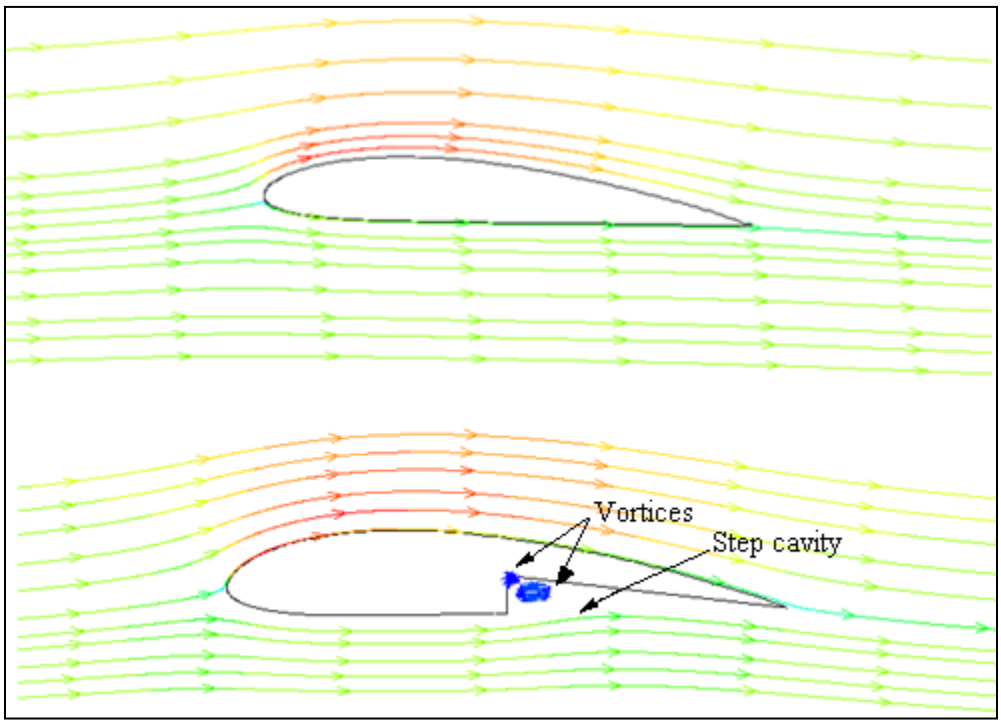

Figure 1-1: Comparison of flow over conventional airfoil and stepped airfoil.

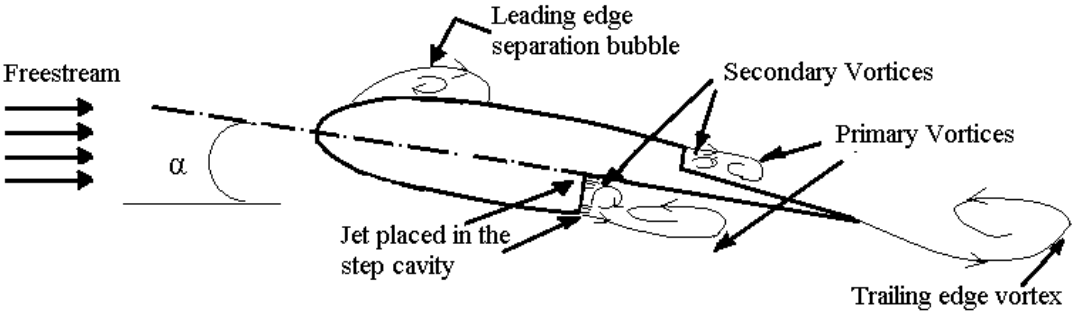

Figure 1-2: Typical flow field around an airfoil with steps on upper and lower edges.

pump aimed at sucking the slow and retarded fluid near the wall thus helping in forming a fresh boundary layer which could be used for avoiding or delaying flow separation. Blowing / Injection flow control technique was used as a part of this investigation.

1.1. LITERATURE REVIEW

Richard L.Kline and Floyd F.Fogleman introduced a breakthrough concept in airfoil design with their stepped airfoils developed in early 1960s. This heralded a new chapter in the aerodynamics with the break-through design of high performance airfoils with extended stalling capabilities and improved lift and drag characteristics. *The Ultimate Paper Airplane*[2] by Richard L.Kline & F.Fogleman (1985, Simon & Schuster) describes that the object of this design was to develop an improved airfoil with enhanced lift, drag and stability characteristics and adaptability over a wide range of speeds, achieved by the generation of vortical flow that alters the flow field resulting in favorable effects. Several other articles published later had also stated that Kline-Fogleman (KF) airfoils were capable of combining the best features of conventional airfoils i.e., better lift with thick ones and higher speeds with thinner ones and further that they worked extremely well for achieving higher lift as well as forward speed. These statements are supported by the world record that Dick Kline still holds for the farthest flying paper plane equipped with stepped airfoils. In addition to the above mentioned claims, in an email that Kline sent to an RC modeling group on issues concerning KF airfoils, he highlighted the advantages of KF airfoils. Most noteworthy ones being the capability of KF airfoils to handle a wide range of speeds; the much greater range for its center of gravity which its case could be moved as much as 40% chord location from the leading edge thus allowing it to carry a heavier load; better air penetration based on the flight experiences of model planes built with KF airfoils; high strength to weight ratio; great stability and control.

Some of the earliest citations of airfoils with vortex trapping cavities were made in a paper by Ringleb F.O.[8] (1961). W.A.Kasper[9] claimed the first successful use of a trapped vortex in a flight experiment in the seventies using a concept so-called as Kasper wing. Experimental studies undertaken by Kruppa[11] (1977) verified that the Kasper-wing produced vortex shedding as against a steady trapped vortex thus resulting in lift enhancement. Some promising results were

obtained by researchers of Saab-Scania (1974) using a wing with a vortex cavity as reported by Kruppa in his paper.

Through the entire period of this research effort at Missouri University of Science and Technology, the biggest question in the minds of researchers was, "Why have the KF airfoils not been used for commercial applications till date even several decades after they were first developed by Kline and Fogleman?" The answers might be found through a set of developments that have taken place over a period of time. According to three independent scientific studies conducted in 1979 at the NASA's Langley Research Center in Virginia, it was concluded that the L/D ratios of wing with KF airfoils weren't encouraging, thus further studies on the wing's resistance to stalling became a low priority. Around the same period of time, Max Davis, of the Air Force Flight Dynamics Lab at Wright-Patterson Air Force Base in Dayton, OH, through his preliminary study stated the Kline-Fogleman wing was not suitable for a full-size aircraft because it had too much drag and not enough lift. In addition to these contradictory theories, the fact that KF airfoils are limited to use in radio-controlled model planes might be one of the reasons why KF airfoils have not been quite a thriving topic of research or their application was not extended to the commercial/defense aviation sectors of aeronautics. One of the objectives of this study to reinforce by the way of sound technical results obtained through both numerical and experimental research and to encompass the application of KF airfoils to a UAV by conducting a case study.

Shifting to the review of studies conducted on stepped airfoils, it was in 1994 that the benefits of KF airfoils were scientifically proven through experiments and flight testing by Demeter G.Fertis[3] when he compared the results obtained for the stepped airfoil with those for conventional NACA 23012 airfoil and confirmed that the airfoils developed by Kline and Fogleman were potential designs to obtain better lift characteristics over a broad range of angles of attack, improve or eliminate stall at all possible operational airspeeds, increase lift to drag ratios over a wider range of operational angles of attack and be adaptable for both fixed and

rotary wing aircraft. This set the direction for a new domain in flow control research, which till then involved focusing on use of flow control techniques on conventional airfoils.

Aerodynamic studies on stepped airfoils were conducted by Stephen Witherspoon[6] and Fathi Finaish (1996) for different configurations defined by the step lengths, depths, and the location of steps on airfoil chord. Experimental tests and numerical investigation with steps on NACA 0012 and 23012 airfoils showed that higher lift coefficients were obtained with lower surface step located at half-chord, extending till the trailing edge at all angles of attack ranging from 0 to 10 deg. Further, upper surface steps located at half-chord and extending till 62.5% chord generated higher L/D ratios when compared with unmodified NACA 0012 airfoil at incidence(s) around 10deg.

BAE SYSTEMS[16], through their "AEROMEMS" research program (2000) concluded that MEMS based fully developed flow control system could result in a timeframe of 10-15 years. Research and Development work was intensified with the launch of "AEROMEMS II" program that focused on extensive wind-tunnel and flight testing of MEMS applications for flow control on a commercial scale. Quality research was also conducted with the initiatives taken at the Air Force Research Laboratory's Air Vehicle Directorate (AFRL/VA), NASA, DARPA apart from the support rendered by technical organizations such as AIAA through The Fluid Dynamics Technical Committee (FDTC) and ASME through The Fluid Dynamics Technical Committee (FDTC).

Research at UCLA/Caltech by Ho[14] and Tai, 2001 involved flight testing of a smart skin attached to an UAV, integrated with several shear stress sensors and balloon actuators distributed over the skin. It was aimed at controlling the pitching, rolling and yawing moments by controlling the position of leading-edge vortices, achieved by micro-actuators coupled with a delta wing boundary layer. T. Crittenden[15], A. Glezer, E. Birdsell and M. Allen used MEMS-based sensing devices and pulse jets integrated into the flow boundary to achieve aerodynamic control.

W.W.H. Yeung[12] (2006) conducted flow visualization studies of corrugated airfoils using steps to compare them with conventional Joukowsky airfoil incorporating a backward facing step based on conformal mapping calculations. The results were in favor of the corrugated airfoils confirming that stepped airfoils produced better lift characteristics due to the formation of vortices. Triple corrugated airfoils produced as much as 10 % more than their conventional counterparts for the same camber, thickness and angle of attack.

Fabrizio De Gregorio and Giuseppe Fraioli[13] (2008) conducted an experimental study of flow control using a trapped vortex cavity on a high thickness airfoil with an objective to apply the results obtained to blended wing designs. Data from PIV measurements showed that passive Trapped Vortex Control (TVC) flow control is neither an effective separation control mechanism nor capable of confining the vortex, and controlling the vortex shedding. On the other hand, active flow control is capable of controlling flow separation.

Masoud Boroomand and Shirzad Hosseinverdi[17] (2009) numerically investigated the turbulent flow around a NACA 2412 airfoil with backward facing steps at high Reynolds number with the objective of enhancing the aerodynamic performance by trapped vortex lift augmentation. All the results obtained through their study were in total agreement with those obtained by Stephen Witherspoon[6] and Fathi Finaish (1996) through their study of NACA 0012 airfoil with a step. Conclusions from their study conducted in 2009 include increase in drag for all stepped airfoil configurations; increase in lift coefficients and lift to drag ratios at some angles of attack for upper step configurations; positive effect shown by lower step configurations on delaying the stalling angle.

1.2. SCOPE OF THE CURRENT STUDY

Vortical flow dominant with swirling vortices resulting from the modification of airfoil geometry forms the basis for the desired flow alteration achievable, which is the prime advantage

of using stepped airfoils while studying them with a goal of enhancement of aerodynamic performance. The resulting flow field around a stepped airfoil has improved lift and/ or reduced drag and produced better stall characteristics, depending on the airfoil configuration and whether or not other flow control techniques are used in conjunction. The study here was aimed at identifying the best setting of steps in the airfoil of choice and making the effective use of vortices resulting from stepped configurations at various flight conditions so as to enhance the aerodynamic performance of airfoil all of which to be achieved using both active and passive flow control techniques discussed in the Introduction Section of this thesis. Numerical studies involved both active and passive flow control techniques while the experimental studies involved the use of only the passive flow control technique. In other words, numerical results were obtained for flow over modified airfoil configurations at different flight conditions to find out whether the usage of step, i.e. whether passive flow control using step produced better results than the conventional NACA airfoil and if it did, the next goal inline was to identify the best configuration while exploring the possibility of use of active flow control on the stepped airfoil with the use of jet placed in the step cavity, i.e. the application of passive and active flow control using a jet placed in the step cavity. Computational Studies were conducted by placing a jet at two different locations to identify the setting that produces the best results with regard to the aerodynamic characteristics of the stepped airfoil configuration studied. Wind tunnel testing was conducted to obtain experimental data for the purpose of validating the results obtained from the numerical studies.

1.3. FORMULATION OF THE FLOW PROBLEM

The flow problem was set up as an airfoil fixed at a certain angle of attack with air flowing over it at a given free stream velocity as illustrated in Figure 1-2. The objective was to enhance the aerodynamic performance of the airfoil using steps and identify the most favorable

step configuration for a given flight condition. The configuration of a step is defined by its location on the airfoil chord, its length and depth expressed in terms of airfoil chord length. The employment of step alone to control the flow field around an airfoil comprises the passive flow control technique used in this study. Figure 1-2 shows the typical flow developments on a modified airfoil with backward facing steps on both the upper and lower surfaces. A jet placed at either of the two locations as mentioned before was used in conjunction with step on the modified airfoil.

1.4. PARAMETER RANGE

There are several parameters which can affect the flow field around an airfoil or a wing in flight. Both the airfoil and step profiles constitute the geometric parameters. The most important ones are the shape of airfoil (symmetric or cambered); chord length; angle of attack; chord-wise location of the step; its length and depth on the upper and /or lower surface. Figure 1-3 shows a sketch of a sample stepped airfoil configuration defining the main geometric parameters. The flow parameters are the free stream velocity, density and viscosity grouped together as the Reynolds number (Re). Re ranges from 0.6 million to 2.5 million for this flow problem while α was varied from 0 to 10 degrees. Based on the results obtained by Stephen Witherspoon and Fathi Finaish (1996), a limited range of parameters were chosen. The airfoil configuration of prime

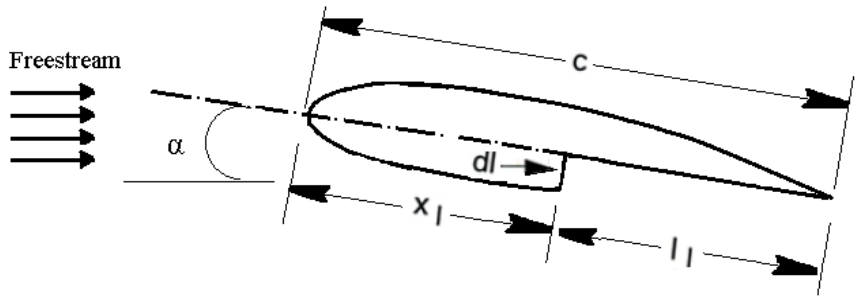

Figure 1-3: Characterization of geometric parameters associated with stepped airfoil studied.

interest was one with the step located on the upper edge at X_l =0.5 with L_l =0.5 and D_l =0.5. NACA 0012 airfoil tested with this step configuration produced higher lift coefficients than the unmodified airfoil for a range of angles of attack varying from 0 to 10 degrees. Thus cases studied were limited to those considering NACA 4415 airfoil as the base airfoil and those with the modified airfoil with a lower surface step located at mid-chord position. The table in the next few sections lists all the major parameters corresponding to each simulation for a set of cases for preliminary study. A jet was used to possibly improve the flow field characteristics and achieve an enhancement in the aerodynamic performance. The jet was characterized by the jet momentum coefficient, Cμ and the jet angle, ζ. The Cμ is the ratio of the product of mass flow rate of the flow through the jet and the jet velocity to the free-stream dynamic pressure as defined below:

$$C\mu = (m_j V_j) / q_\infty \quad (1)$$

The Cμ was varied from 0.00027 to 0.01731 while the jet angle was varied in increments of 15 degrees from 0° to 45°.

2. METHODS OF INVESTIGATION

Studies involving investigation of stepped airfoils with/without using jets were carried out using both computational and experimental approaches to examine the associated flow field developments and the resulting aerodynamic forces. The numerical studies were conducted using a commercially available computational fluid dynamics package to simulate flow around the airfoils. The latter part of the research was conducted by employing a wind tunnel for running tests on the airfoils studied numerically to generate some quantitative and qualitative data for validating the numerical results. This approach required building a test wing model using a conventional NACA airfoil and redesigning it to obtain the modified airfoil configurations to be tested. Force data including lift and drag were recorded during the tests. Experimental studies were conducted to complement the results obtained by the computational studies. Besides this, they were sought to provide information for a better understanding of the complex flow physics involved with the stepped airfoils.

2.1. COMPUTATIONAL APPROACH

2.1.1. Governing Equations. The three fundamental principles governing the fluid flow characteristics are the conservation of mass, conservation of momentum, and conservation of energy. As there is no heat addition or rejection involved in this investigation, the conservation of energy principle is not discussed in this section. The conservation of mass principle applied to a fluid element in a fixed control surface is given by the following equation

$$\frac{\partial \boldsymbol{\rho}}{\partial \boldsymbol{t}} + \boldsymbol{\nabla} \cdot (\boldsymbol{\rho V}) = \mathbf{0} \tag{2.1}$$

where $\boldsymbol{\nabla}$ is the gradient operator defined as

$$\boldsymbol{\nabla} \equiv \left\{ \boldsymbol{i}\frac{\partial}{\partial x} + \boldsymbol{j}\frac{\partial}{\partial y} + \boldsymbol{i}\frac{\partial}{\partial z} \right\} \tag{2.2}$$

The momentum equation is obtained by applying the Newton's second law of motion to a fluid element passing through a fixed control surface. It is expressed as below.

$$\frac{\partial(\rho V)}{\partial t} + \boldsymbol{\nabla} \cdot \boldsymbol{\rho VV} = \boldsymbol{\rho f} + \boldsymbol{\nabla} \cdot \boldsymbol{\Pi}_{ij} \tag{2.3}$$

The first term in the above equation defines the rate of change of momentum in the control surface; the second term defines the rate of loss of momentum by convection through the control surface. The first term on the right-hand side of (2.3) represents the body force while the second term represents the surface forces resulting from the normal and shear stresses defined as

$$\boldsymbol{\Pi}_{ij} = -\boldsymbol{P}\boldsymbol{\delta}_{ij} + \boldsymbol{\tau}_{ij} \tag{2.4}$$

$$\boldsymbol{\tau}_{ij} = \boldsymbol{\mu}\left[\left(\frac{\partial \boldsymbol{u}_i}{\partial \boldsymbol{x}_j} + \frac{\partial \boldsymbol{u}_j}{\partial \boldsymbol{x}_i}\right) - \frac{\mathbf{2}}{\mathbf{3}}\boldsymbol{\delta}_{ij}\,\frac{\partial \boldsymbol{u}_k}{\partial \boldsymbol{x}_k}\right] \quad \boldsymbol{i,j,k} = \mathbf{1,2,3} \tag{2.5}$$

where $\boldsymbol{\delta}_{ij}$ is the Kronecker Delta function ($\boldsymbol{\delta}_{ij} = \mathbf{1}\ \boldsymbol{if}\ \boldsymbol{i} = \boldsymbol{j}$) ;($\boldsymbol{\delta}_{ij} = \mathbf{0}\ \boldsymbol{if}\ \boldsymbol{i} \neq \boldsymbol{j}$).

$\boldsymbol{u}_i$ and $\boldsymbol{x}_i$ represent the three components of the velocity vector *V* and the position vector respectively. Applying (2.4) and (2.5) to (2.3), it can be expressed as below.

$$\boldsymbol{\rho}\frac{\boldsymbol{DV}}{\boldsymbol{Dt}} = \boldsymbol{\rho f} - \boldsymbol{\nabla P} + \frac{\partial}{\partial \boldsymbol{x}_j}\left[\boldsymbol{\mu}\left(\frac{\partial \boldsymbol{u}_i}{\partial \boldsymbol{x}_j} + \frac{\partial \boldsymbol{u}_j}{\partial \boldsymbol{x}_i}\right) - \frac{\mathbf{2}}{\mathbf{3}}\boldsymbol{\delta}_{ij}\boldsymbol{\mu}\,\frac{\partial \boldsymbol{u}_k}{\partial \boldsymbol{x}_k}\right] \tag{2.6}$$

The Navier–Stokes equations discussed in the momentum equation above are complex partial differential equations which by themselves are difficult to solve without making any sort of approximations. Thus in modeling a turbulent flow, time-averaged flow variables are used in the form of the Reynolds Averaged Navier–Stokes (RANS) equations to obtain approximate solutions to flow problems. To obtain the RANS equations the flow variables in the conservation equations are split into the mean (constant) and fluctuating (time-varying) component and the entire equation is averaged with respect to time. In the turbulence-modeling of a fluid flow, the

flow variables of velocity, pressure, and temperature can be expressed as

$$\boldsymbol{u} = \overline{\boldsymbol{u}} + \boldsymbol{u}' \qquad \boldsymbol{v} = \overline{\boldsymbol{v}} + \boldsymbol{v}'$$

$$\boldsymbol{P} = \overline{\boldsymbol{P}} + \boldsymbol{P}' \qquad \boldsymbol{T} = \overline{\boldsymbol{T}} + \boldsymbol{T}' \tag{2.7}$$

where u and v represent the *x* and *y* components of the velocity vector respectively. The continuity equation can now be modified as

$$\frac{\partial \overline{\rho}}{\partial t} + \nabla \cdot \overline{\rho \boldsymbol{V}} = \mathbf{0} \tag{2.8}$$

and the modified momentum equation can be expressed as

$$\overline{\rho}\frac{D\overline{V}}{Dt} = -\nabla \overline{P} + \frac{\partial}{\partial x_i}\left[\mu\left(\frac{\partial u_i}{\partial x_j} + \frac{\partial u_j}{\partial x_i}\right) - \overline{\rho u_i' u_j'}\right] \tag{2.9}$$

An additional transport equation is required to solve the RANS equations discussed above. The transport equation used in this investigation is the Spalart-Allmaras model defined below.

$$\frac{\partial(\rho\hat{\nu})}{\partial t} + \frac{\partial(\rho\hat{\nu}u_i)}{\partial x_i} = \boldsymbol{G_\nu} + \frac{1}{\sigma_{\hat{\nu}}}\left[\frac{\partial}{\partial x_j}\left\{(\mu + \rho\hat{\nu})\frac{\partial \hat{\nu}}{\partial x_j}\right\} + C_{b2}\,\rho\left(\frac{\partial \hat{\nu}}{\partial x_j}\right)^2\right] - \boldsymbol{Y_\nu} + \boldsymbol{S_{\hat{\nu}}} \tag{2.10}$$

This one-equation model solves for the kinematic eddy or turbulent viscosity. $\boldsymbol{G_\nu}$ represents the production of turbulent viscosity; $\boldsymbol{Y_\nu}$ represents the destruction of turbulent viscosity that occurs due to wall blocking and viscous damping; $\boldsymbol{\nu}$ is the kinematic viscosity; $\hat{\boldsymbol{\nu}}$ is a variable identical to the turbulent kinematic viscosity accept in the near-wall region which is affected by viscosity. $\boldsymbol{S_{\hat{\nu}}}$ is the user-defined source term while $\boldsymbol{\sigma_{\hat{\nu}}}$ and $\boldsymbol{C_{b2}}$ are constants.

2.1.2. Tools Used. All of the computational work was done using commercial software packages. All the Pre-processing comprising mesh generation, quality control and setting up of the boundary conditions was done using GAMBIT. "GAMBIT 2.4" was used for generating meshes for all the airfoil configurations. The meshes were then imported into ANSYS

12 - “FLUENT”, a finite volume method based CFD tool which solves the governing equations of conservation of mass and momentum was the flow solver used for the entire numerical analysis. Post processing including generation of plots and figures was done using FLUENT and Tecplot.

2.1.3. Computational Details. The problem was set up as a two dimensional flow problem in single phase. The Cartesian co-ordinate axes were fixed at the leading edge of the airfoil in each case. The computational domain comprises of four blocks for all base airfoil configurations, while the single step configurations had eight mesh blocks. The blocks encompassed a region of length three chords above and below the X-axis which coincides with the chord line of the airfoil, 2.5 chords ahead of the leading edge and 4 chords behind the trailing edge as shown in Figure 2-1. For the most basic mesh or the coarsest mesh with the base airfoil, the grid density within the blocks was 45 cells above and below the X-axis normal to the airfoil surface distributed in a successive ratio of 1.15, concentrated near the airfoil surface. In the chord-wise direction, the flow domain was meshed with 60 nodes concentrated near the airfoil trailing edge. The mesh becomes coarser towards the end of the flow domain to take advantage of the property of fully developed flow farther away from the airfoil. The upper and lower edges of the airfoil are split to distribute the mesh points resulting in a mesh of better quality. Both the edges of the airfoil meshed with 76 nodes. Figure 2-2 shows the grid distribution around a NACA 4415 airfoil with a step.

The flow was modeled as steady, incompressible in the flow domain comprising several blocks. The fluid chosen was air at standard atmospheric conditions which were set as the reference values along with the free-stream velocity set corresponding to the flow Re for each simulation run for the preliminary cases of study. The inlet was set as “Velocity Inlet” which includes all the front, top and bottom edges of the flow domain. The x and y-velocities are “u”, which is defined by the Reynolds number used and “v” that equals 0 m/s. “Spalart-Allmaras” one

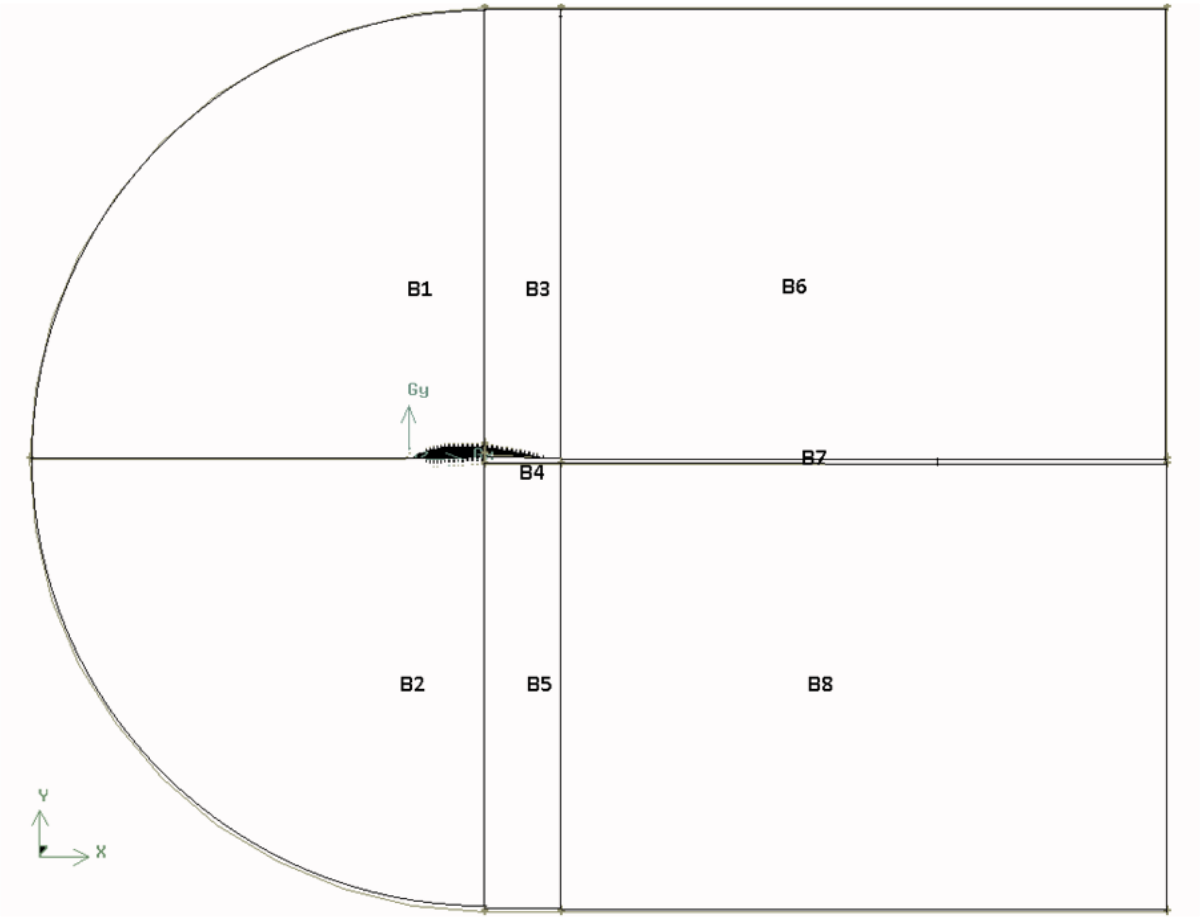

Figure 2-1: Block structure of the flow domain over an airfoil with a step on the lower surface.

equation turbulence model was used in FLUENT for all computations. This computational model is well suited for modeling wall driven flows which transpire most commonly over aerodynamic bodies.

All the exit boundaries combined were set as “Pressure Outlet”. All the airfoil edges together were set as “Wall” with no-slip condition. The convergence criteria was set at 1e-06 for residuals, continuity, x and y velocities uniformly. The flow solver used the SIMPLE algorithm for pressure-velocity coupling. Least Squares Cell Based method was used for gradient computations. Pressure was set as second order, Momentum, and Modified Turbulent Viscosity were set as Second Order Upwind for Spatial Discretization computations.

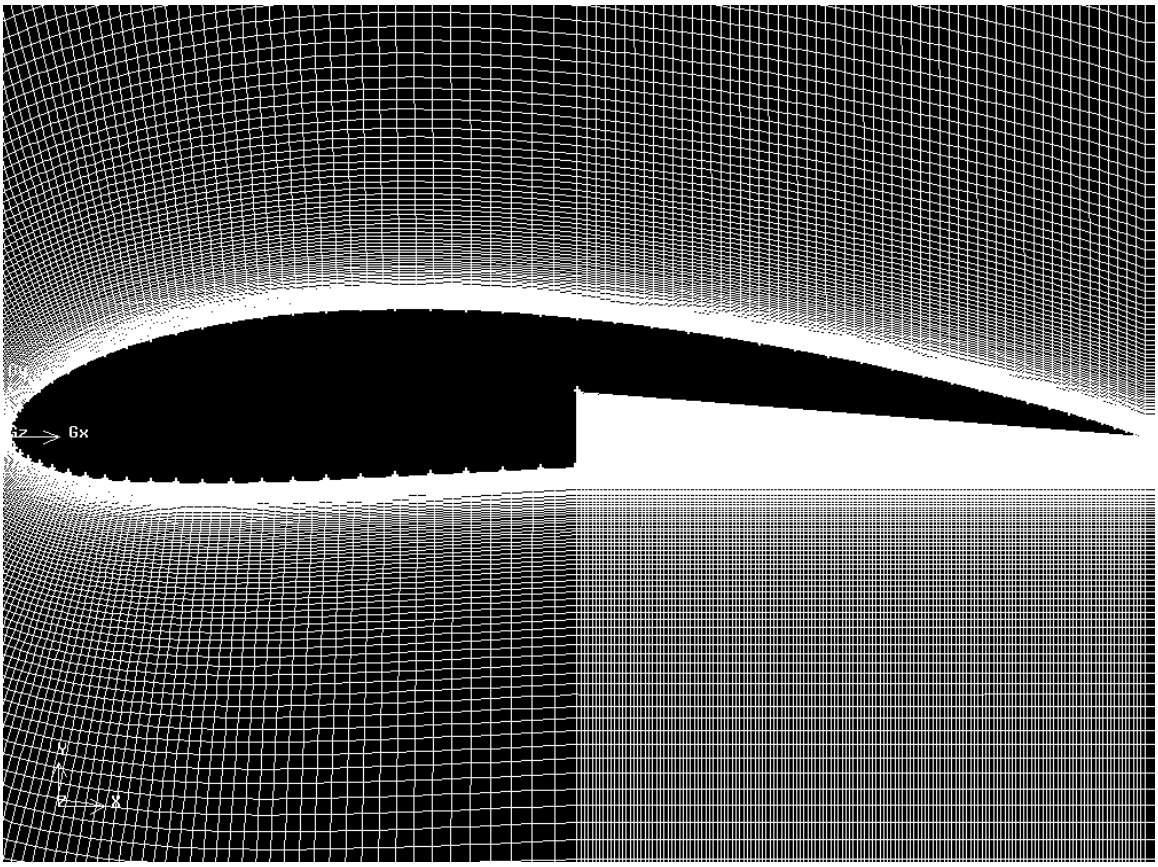

Figure 2-2: Grid distribution around a NACA 4415 airfoil with a step on the lower surface.

2.1.4. Grid-Convergence Study. Since the grid densities normal to parallel to the flow direction and fineness of the mesh near the airfoil surface can affect the accuracy of the solution, the effect of these parameters was studied so that results did not deviate much as the mesh size was increased. The mesh size in terms of number of nodes was increased in "n" multiples and the simulations were run for each case till the converged results were close to those obtained with previous mesh size. This way study was done till the grid convergence was reached and the best mesh configuration was identified beyond which the results do not vary with the grid density of the mesh points. Also during the study the results obtained in each case were compared with the experimental data available to identify the mesh generating the most accurate results bearing in mind the grid quality in each case. Figure 2-2 illustrates the mesh around a NACA

4415 airfoil with a step. As shown by the figure, the grid is much finer near the edge of the airfoil and grid points are concentrated in the step cavity to obtain more accurate results as well as better resolution of the flow field near the airfoil edge and in the step cavity. The final refined meshes around the base airfoil had around 95,000 grid points, while the meshes for stepped airfoil cases had about 120,000 grid points. The other meshes for cases of jet placed in the step cavity around 150,000 points each. Figure 2-3 shows the grid convergence for the lift and drag coefficients.

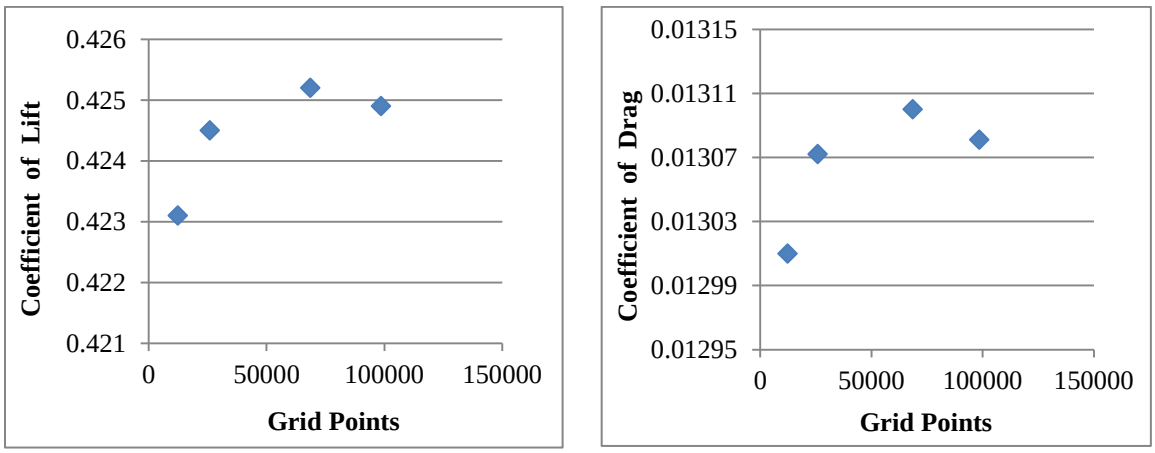

Figure 2-3: Illustration of Grid Convergence for the lift and drag coefficients.

2.1.5. Preliminary Results. Some initial numerical results obtained were compared with the experimental data available in Reference 10 in order to evaluate the validity of the results as tabulated in Table 2-1. As the Reynolds numbers used were of the order of millions, all the computations were performed considering the flow to be turbulent. The initial results generated especially in the case of lift computations for the Reynolds number of three million were in descent agreement with the experimental data. Figure 2-4 compares experimental data available with the preliminary numerical results for the cases studied. The error lies within 5-10 % as compared with the experimental values of lift, while the corresponding error for drag values is

Table 2-1: Summary of NACA 4415 airfoil configurations studied for validation.

Case No	Airfoil Configuration	Re	U_∞ [m/s]	α [deg.]
1	Base	3 e 6	43.61	0
2	Base	3 e 6	43.61	4
3	Base	3 e 6	43.61	8
4	airfoil with step	3 e 6	43.61	0
5	airfoil with step	3 e 6	43.61	4
6	airfoil with step	3 e 6	43.61	8

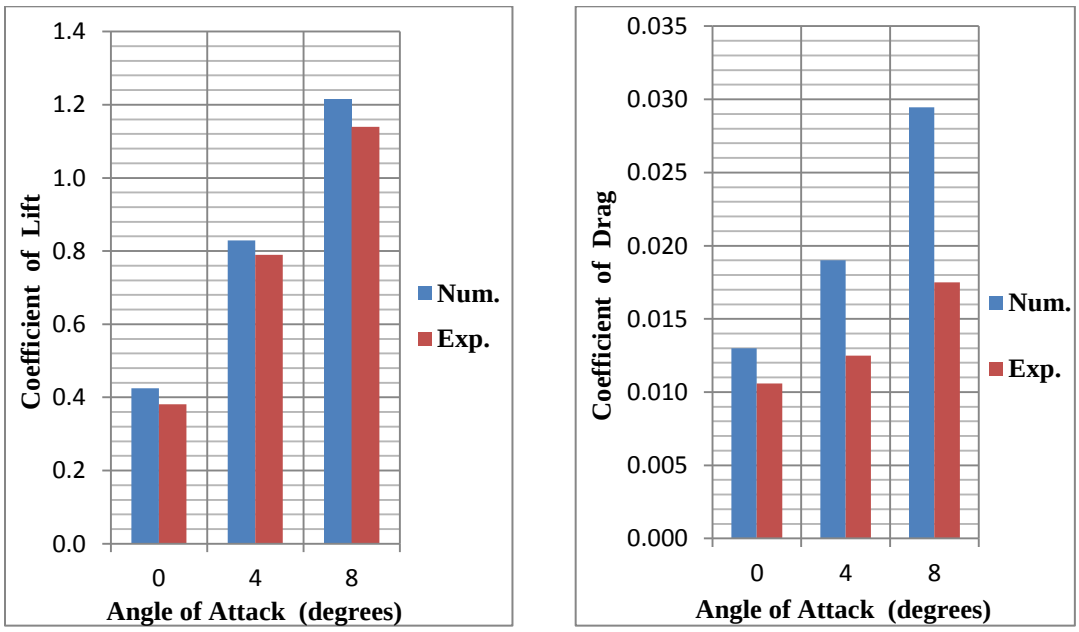

(a). (b).

Figure 2-4: Comparison of numerical results with experimental data. (a) Lift; (b) Drag

higher lying between 23-65 %. As there is high error in the drag results obtained, the author would like to caution researchers that the accuracy of the quantitative results presented in this thesis may not be highly reliable. On the other hand if the error in the drag results were to be much less of the order of the error in the lift data, then the values of lift to drag ratio presented in this thesis would be much higher which is beneficial. Use of the results for future studies may be made while being conscious about these observations. Preliminary results were obtained for

NACA 4415 airfoil at three different angles of attack (0°, 5°, and 10°). Also results were also obtained for modified airfoil with step at these α(s) to examine whether use of step yielded better aerodynamic performance measured in terms of the L/D ratio, the higher the better. As expected, L/D ratios for the stepped airfoils were higher than those for the base airfoils. All the six cases mentioned above constitute the ones studied for validating the computational results.

2.2. EXPERIMENTAL APPROACH

The second part of this research involved experimental investigation of stepped airfoils to validate some of the results obtained with numerical studies conducted as a part of this research effort. All the experimental studies were conducted in the Aerospace Flow Laboratory located in the Department of Mechanical and Aerospace Engineering [MAE] at the Missouri University of Science and Technology. The flow lab at Missouri S & T houses the wind tunnels used for aerodynamic testing along with the test model fabrication facilities. This section presents the approach followed for the wind tunnel testing of the modified NACA 4415 airfoil with lower surface step.

2.2.1. Wind Tunnel Facility. The Aerospace Flow Laboratory at Missouri S & T houses a subsonic wind tunnel which was used for all the testing done as a part of the current research to measure the airfoil force data This facility has an open return type wind tunnel. The tunnel is equipped with three interchangeable test sections that can easily be installed downstream of a convergent section. A computer station equipped with an experimental data acquisition system is available for recording data. The aerodynamic forces on the test models were measured for a range of tunnel speeds corresponding to Re's ranging from 0.4 million to 0.8 million on the model that was tested based on the conditions of pressure and temperature in the wind tunnel that were measured during the tests. The tunnel consists of a bell-mouth inlet, a honeycomb structure,

a settling chamber, and a 6:25:1 fiberglass/foam lamination contraction. Flow turbulence is controlled by a combination of three anti-turbulence screens and the honeycomb panel installed in the tunnel settling chamber. Figure 2-5 depicts a sketch of the wind tunnel and the flow visualization system used. These sections are followed by an 18" x 18" x 60" Plexiglas test section, and a diffusor. The tunnel, driven by a 20 hp DC motor that provides feedback control for a tubular accoustafoil fan, is capable of a maximum flow velocity of 68 mph (or) 30.5 m/s. The tunnel is equipped with a smoke rake located upstream of the settling chamber section in the tunnel. The rake is connected to a pressurized tank fed by a Rosco fog generator, which produces the fog/smoke by heating Rosco fog fluid. A pressure regulator on the tank and a fog volume control on the generator allow for optimal adjustment of the smoke sheet as per the test model size and/or tunnel speed. A still camera was used to record the images and a basic lighting system was available for illuminating the test section during the testing. The test model in the wind tunnel was supported using a piece of copper tubing passing through holes made in the test section walls and the test model. The ends on the tubing rested on the load cells. One end of the tubing was fitted with a mechanism to alter the angle of attack the test model during the testing. aerodynamic forces acting on the model were measured using these load cells. The load cells are capable of measuring forces between 0.0015 kg and 5 kg. The other end is connected to the data

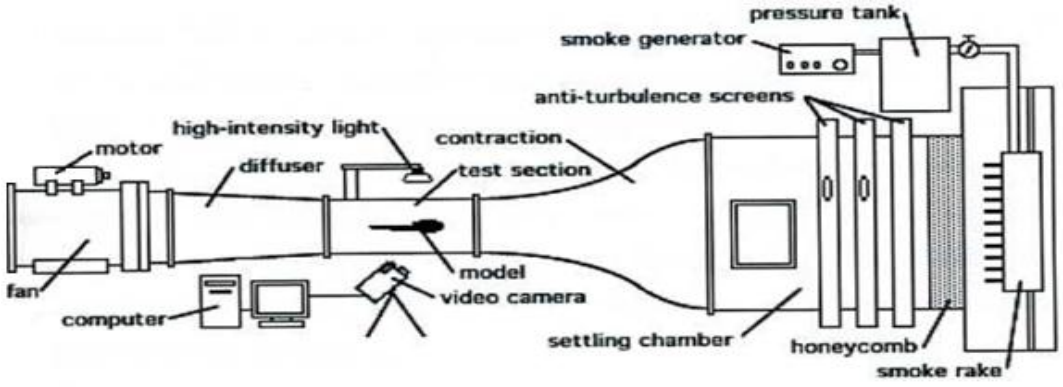

Figure 2-5: Schematic of the wind tunnel and flow visualization facility. Courtesy: MAE Dept.

acquisition system used for recording the force data.

2.2.2. Test Model. The wing model used for wind tunnel testing was built with a step whose depth could be varied remotely during the testing. This mechanized wing model consisted of wing sections employing the NACA 4415 airfoil with a lower surface step configuration of X_l =0.5, L_l =0.5, and a variable depth. The chord of the square plan form model was 16 inches while the span was 16 inches resulting in a surface area of 1.78 ft^2. The span of the model allowed for only 1 inch of clearance between the model and the wind tunnel on either side so that the flow could be assumed to be entirely two dimensional. The model was fabricated using a 1/8" thick sheet of balsa wood for the wing sections, a 1/16" thick balsa sheet for outer sheeting, 1" x 3/8" spruce for spars, 1/8" aluminum sheet for the variable lower surface step. During the testing, the step was actuated using a remote controllable mechanism involving a servo motor fitted within the model using a set of plastic linkages. The various step depths were marked in black ink on the wing-tip airfoil made of Plexiglas for easy detection during the testing. The servo motor was fitted onto the balsa framework inside the wing. To facilitate easy access to the motor and the wiring, an access plate was designed and fabricated out of a 1/8" balsa sheet and then filed to give it a smooth finish so its upper surface matches with the contour profile of the rest of the wing surface. It was then screwed in place onto the framework. Figures 2-6 (a), (b), (c), and (b) show the set of NACA 4415 airfoils made, wing framework, servo and step surface linkage mechanism, perspective view of the model with the access plate and the servo motor mounted on a set of wing ribs. The step-activating mechanism was operated using a transmitter remotely. The model was mounted with the step fully retracted so that the model could be assumed to be corresponding to the conventional NACA 4415 airfoil considered the base airfoil for all the cases. During the testing, the step depth was varied gradually to record the experimental data for each modified airfoil configuration of X_l =0.5, L_l =0.5, and the particular step depth setting.

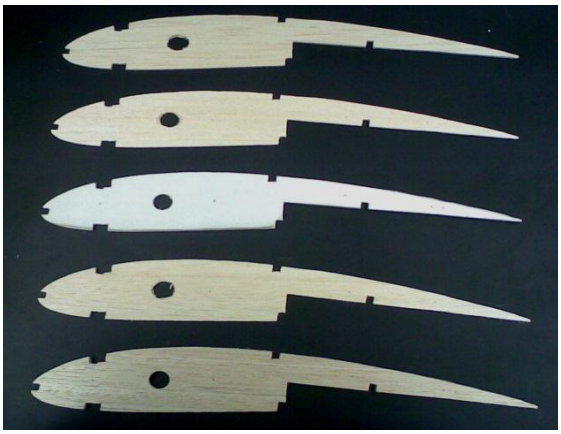

(a).

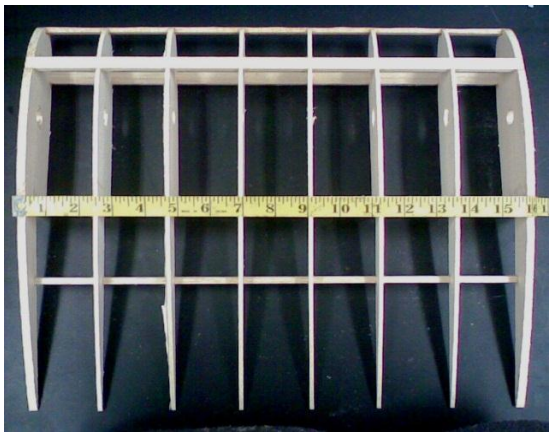

(b).

(c).

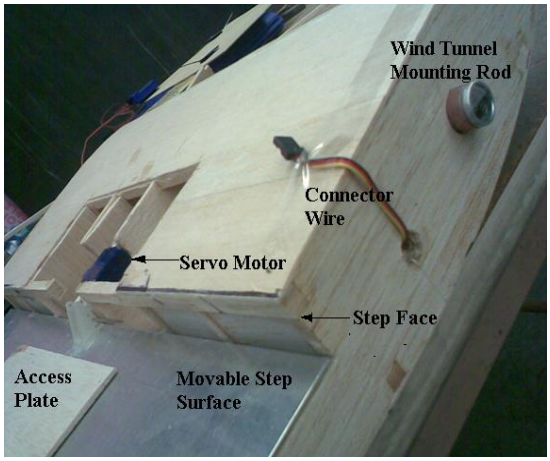

(d).

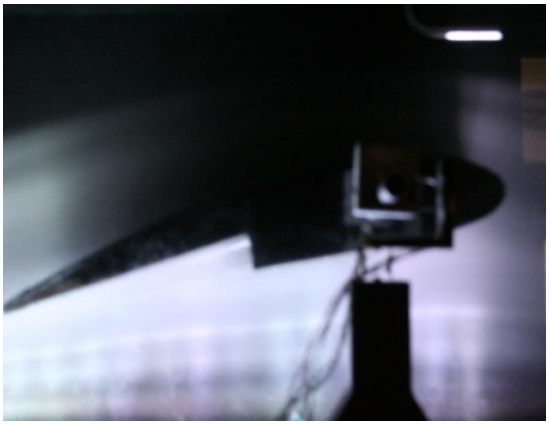

(e).

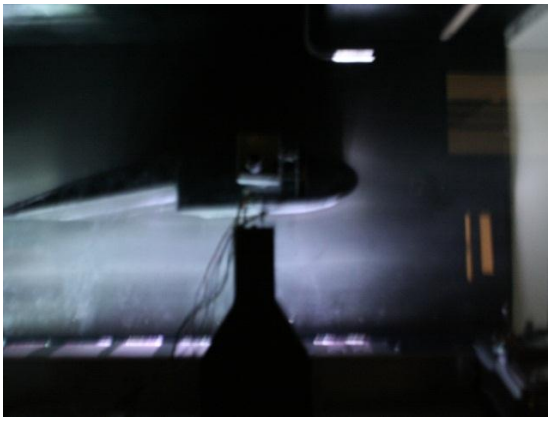

(f).

Figure 2-6: Illustrations of the test model. (a) NACA 4415 airfoils; (b) wing framework; (c) servo and step surface linkage; (d) perspective view of the wing model; (e) model mounted in the test section; and (f) lighting system inside the test section.

3. RESULTS AND DISCUSSION

Through numerical studies and experimental investigation, useful results were generated for airfoil configuration comprising of conventional NACA airfoil and the corresponding modified airfoil with step introduced on the lower surface. This section presents the comprehensive description and analyses of all the usable results obtained. Results are presented for airfoils by varying some geometric and aerodynamic parameters along with discussion of the results with regard to the flow structures discussed in the first chapter of this thesis, pressure distribution, and aerodynamic characteristics associated with the modified NACA 4415 airfoil configuration set at a predefined attitude and a given set of inlet conditions. The numerical results obtained were used to compare the various stepped airfoil cases with the corresponding cases using jet by varying the jet parameters. Further, this section presents the results comprising the experimental force measurements leading to aerodynamic coefficient data.

3.1. COMPUTATIONAL RESULTS

Results showing the flow field developments are presented as velocity vector, static pressure contour and pressure coefficient plots using FLUENT and Tecplot as post processors. Further, aerodynamic characteristics such as lift, drag and pitching moment coefficients are also presented as obtained from the resulting pressure and shear stress distributions at different flight conditions. Conventional NACA 4415 airfoil and the modified airfoil configuration were evaluated for a given set of inlet conditions. On the basis of the results generated by Stephen Witherspoon[5] and Fathi Finaish (1996) according to which airfoil with step on the lower edge with X_l =0.5, L_l =0.5, and D_l =0.5 is the best in terms of aerodynamic performance, further analysis was sought for the cambered NACA 4415 airfoil. Table 3-1 enlists the various cases investigated numerically as a part of this research. The operating conditions matching the

standard atmospheric values of pressure, temperature, and density were kept the same for all the cases during the study.

3.1.1. Passive Flow Control. In this study, this flow control technique involves the use of step to modify the flow field around a NACA 4415 airfoil. The resulting airfoil configuration brings about some flow field developments which might help control the flow so as to enhance the aerodynamic performance.

Table 3-1: Summary of NACA 4415 airfoil configurations studied.

Case No	Airfoil Configuration	Re	U_∞ [m/s]	α [deg.]
7	Base	1.7 e6	24.93	2
8	X=0.5; D=0.5; L=0.5	1.7 e6	24.93	2
9	Base	0.6 e6	8.76	4
10	X=0.5; D=0.5; L=0.5	0.6 e6	8.76	4
11	Base	1.2 e6	17.50	4
12	X=0.5; D=0.5; L=0.5	1.2 e6	17.50	4
13	Base	1.8 e6	26.40	4
14	X=0.5; D=0.5; L=0.5	1.8 e6	26.40	4
15	Base	2.5 e6	37.53	8
16	X=0.5; D=0.5; L=0.5	2.5 e6	37.53	8

3.1.1.1. Velocity contours and streamlines. In order to explore the flow field developments around a NACA 4415 airfoil with a step, let us start by considering a sample velocity contour and streamline plot. Figure 3-1 shows a global view of the streamlines and velocity contour field around airfoil with step configuration of X_l =0.5, L_l =0.5, and D_l =0.5 on the lower edge. Figure 3-2 presents the pressure contours for the same configuration. The legend Figure 3-1 shows the velocity contours colored by magnitude of velocity in meters per second,

where the free stream velocity is 26.4 m/s corresponding to a Re of 1.8 million. The angle of attack is 4 degrees. In the figure it can be seen that as the flow progresses, it accelerates over the front portion of the airfoil, slightly decelerating past the quarter chord leaving a wake behind the trailing edge of the airfoil. Figure 3-3 shows the magnified view of the flow inside the region of stepped airfoil shown in Figure 3-1 along with the plots for cases of Re = 0.6 million and 1.2 million. As can be noticed, the flow separates at the leading edge of the step forming a vortex behind the step face and then reattaches itself some distance downstream. A secondary vortex is formed after the reattachment near the top step corner as shown. The secondary vortex is much smaller than the primary one. Recirculation zones are clearly shown in the figure, which are similar to the predicted flow developments illustrated in Figure 1-2. Though the step extends till the trailing edge, the center of the primary vortex occurs closer to the step face as can be seen in Figure 3-1. Figures showing velocity contour and streamline plots for the modified airfoil with lower edge step configurations of X_l =0.5, L_l =0.5, and D_l =0.5 at $\alpha = 4°$ and at Re(s) of 0.6, 1.2, and 1.8 million are grouped together. Also figures showing velocity contour and streamline plots for the same airfoil configurations at $\alpha = 8°$ at Re of 2.5 million and at $\alpha = 2°$ at Re of 1.7 million are grouped together. The legend on all the velocity contour and streamline plots defines the dimensionless velocities represented by the colored vectors defined as:

$$v = V/ U_{\infty}, \text{ where } V = [(\text{X-Velocity})^2 + (\text{Y-Velocity})^2]^{1/2} \quad (3.1)$$

With the increase in Re, the overall flow velocities in the flow field will be higher. But the strength of the vortices may not be high enough for all the stepped cases for any benefit in terms of the aerodynamic characteristics in each and every case which is discussed further in the later sections. Higher inlet velocities produce stronger vortices in the step region thus allowing the possibility of producing better lift characteristics which to prove is one of the goals in this study.

From the plots in Figure 3-3, not much variation can be seen as the Re is increased. There is a slight variation in the velocity contour plots shown in Figure 3-4 in comparison with those in the Figure 3-3. Figure 3-5 shows the plots illustrating the vorticity distributions for the various cases studied at $\alpha = 4°$. As can be noticed from the plots, the vorticity gradients within the step cavity increase as the Re is increased. The increase in the vorticity gradients is also clear from the Figure 3-6. As there is a consistent rise in drag for the modified airfoils over the base airfoil cases, the focus of this study was to identify the benefits in terms of the lift to drag ratios. The corresponding results are discussed in the section of aerodynamic coefficients.

3.1.1.2. Pressure distributions. The effect of these flow developments on the pressure around the airfoils and the resulting aerodynamic characterisitics can be better understood by analyzing the plots of static pressure contours which are curves along which the pressures are equal. Figure 3-2 shows a global view of pressure contours around the airfoil configuration of Figure 3-1. The legend indicates values of pressure expressed as pressure coefficient C_p varying from -2.5 to 1. Figures 3-7 and 3-8 contain the pressure contour plots corresponding to the velocity vector plots grouped together as mentioned earlier for the same set of parameters. The C_p varies from -1.3 to 1 on all these plots showing the magnified view of the pressure distribution within the step cavity. The recirculation in the step cavity due to the formation of vortices can be seen as concentric circles of pressure contours with their center coinciding with the center of the vortex. Regions with denser spacing of pressure contours are indicative of stronger pressure gradients and vice-versa. These intense regions can be visualized downtream of the vorex where there is reattachement of flow and thus a pressure gain. Also regions near the airfoil leading edge and the upper side of the front portion have high pressure gradients. It can be observed that there is high pressure at the leading edge due to flow stagnation. As the flow passes over the convex upper portion, there is decrese in pressure due to the flow

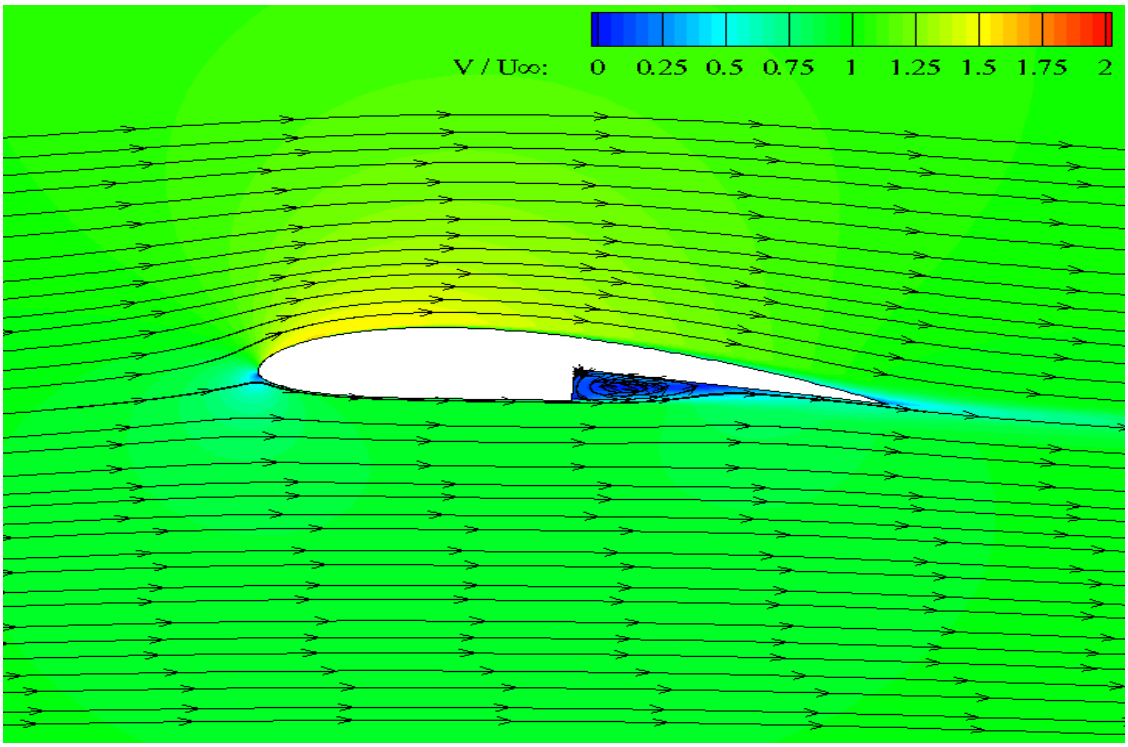

Figure 3-1: Global View of Velocity Contours and Streamlines around a stepped NACA 4415 airfoil at $\alpha = 4°$; Re = 1.8 million; X_l =0.5; L_l =0.5; and D_l =0.5.

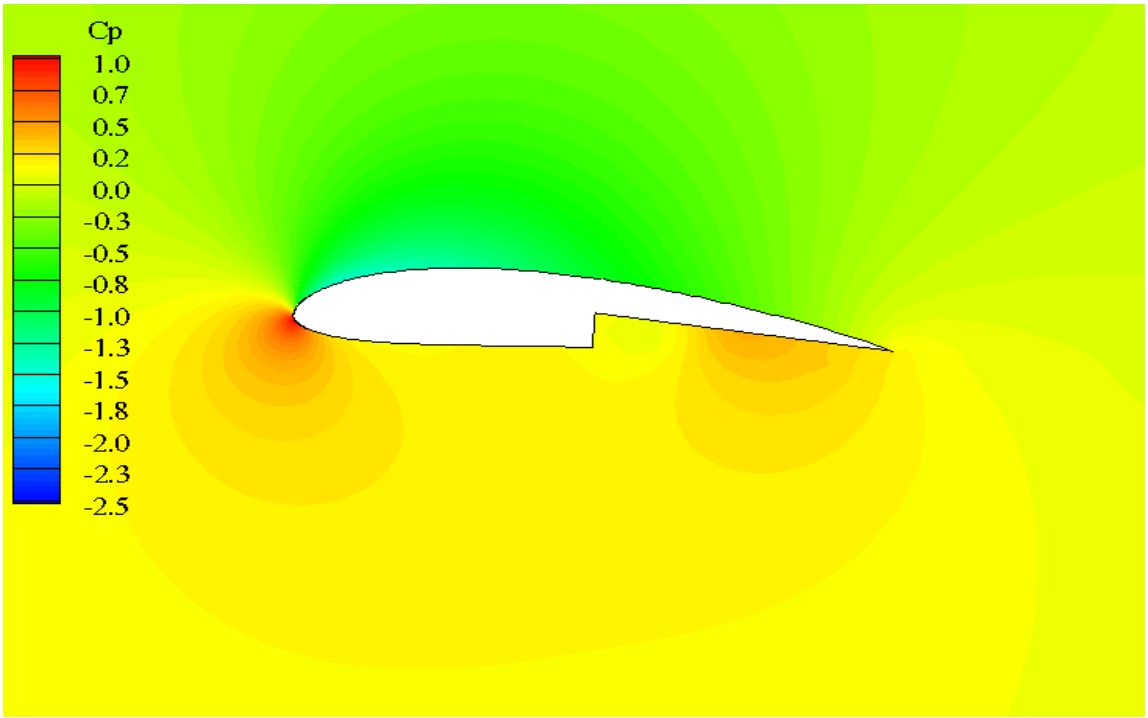

Figure 3-2: Global View of Pressure Contours around a stepped NACA 4415 airfoil at $\alpha = 4°$; Re = 1.8 million; X_l =0.5; L_l =0.5; and D_l =0.5.

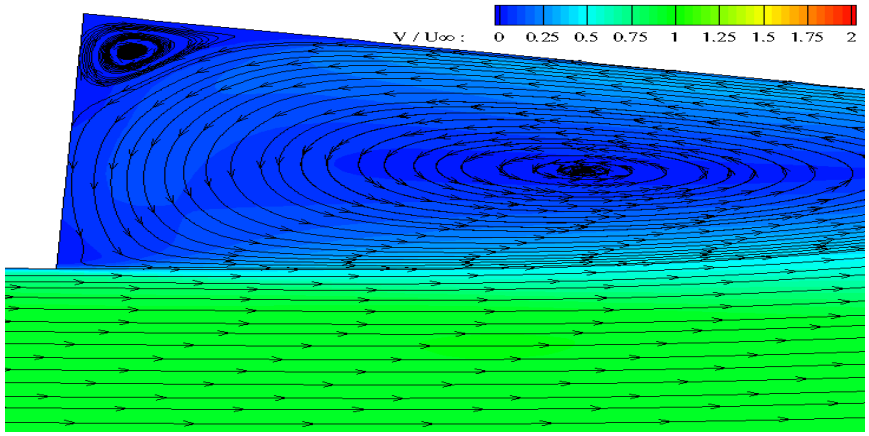

(a).

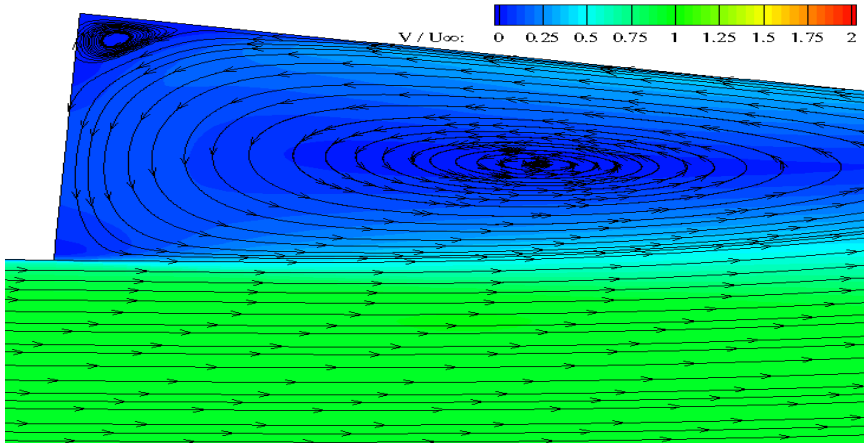

(b).

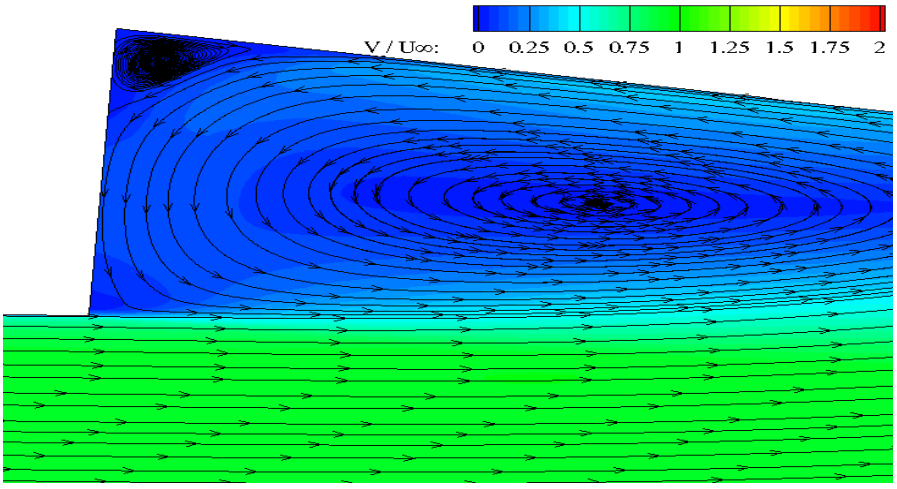

(c).

Figure 3-3: Velocity Contours and Streamlines in the step cavity of a modified NACA 4415 airfoil at $\alpha = 4°$; $X_l = 0.5$; $L_l = 0.5$; and $D_l = 0.5$. (a) Re = 0.6 million; (b) Re = 1.2 million; (c) Re = 1.8 million.

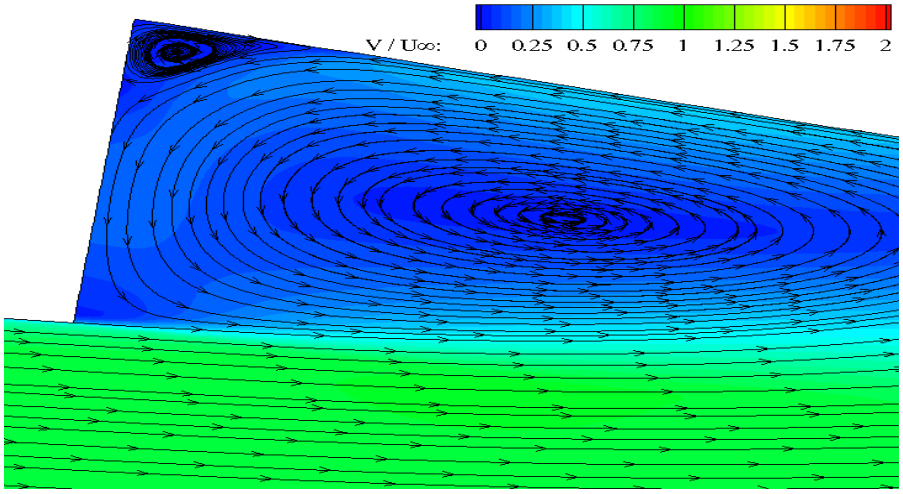

(a).

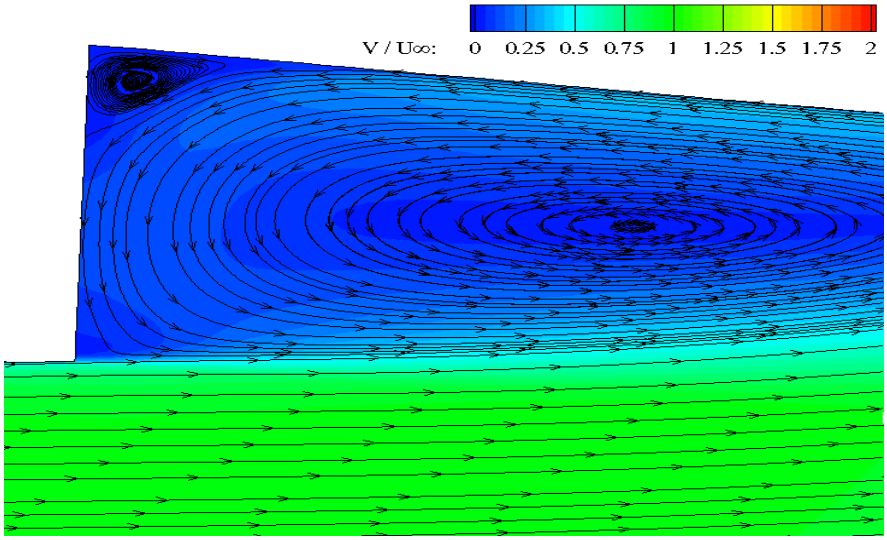

(b).

Figure 3-4: Velocity Contours and Streamlines in the step cavity of a modified NACA 4415 airfoil; X_l =0.5; L_l =0.5; and D_l =0.5. (a) $\alpha = 8°$, Re = 2.5 million; (b) $\alpha = 2°$, Re = 1.7 million.

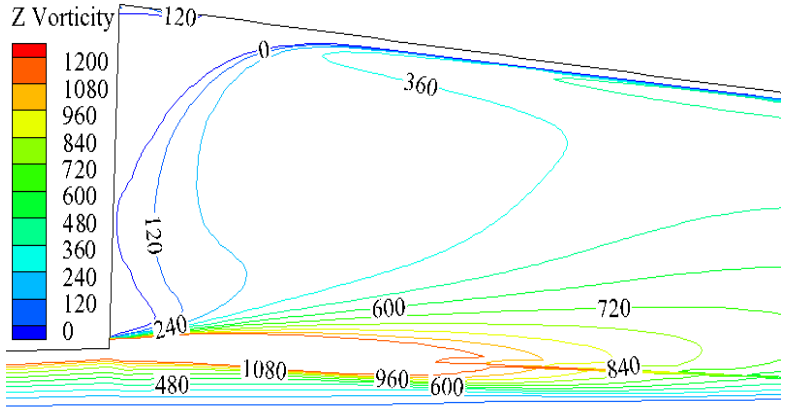

(a).

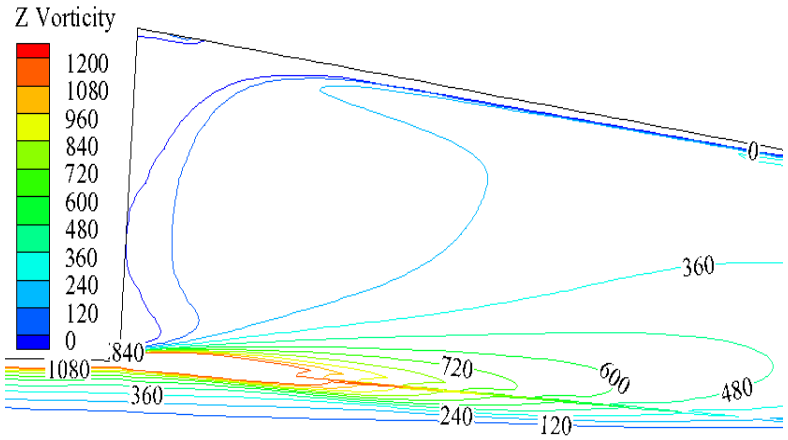

(b).

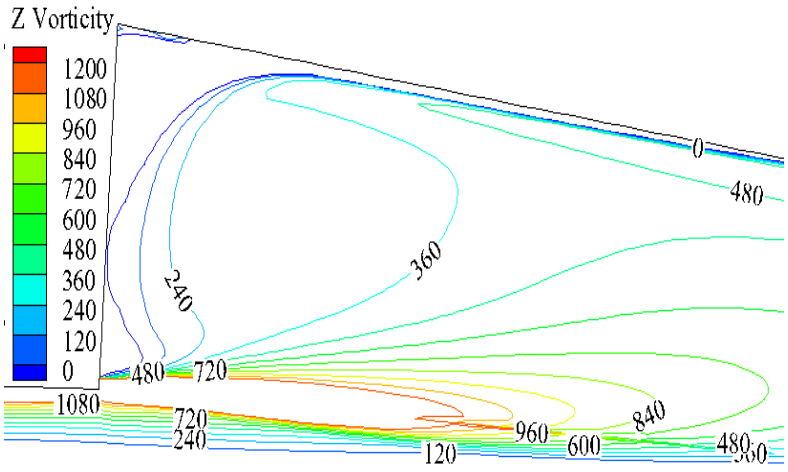

(c).

Figure 3-5: Vorticity Contours in the step cavity of a modified NACA 4415 airfoil at $\alpha = 4°$; $X_l = 0.5$; $L_l = 0.5$; and $D_l = 0.5$. (a) Re = 0.6 million; (b) Re = 1.2 million; (c) Re = 1.8 million

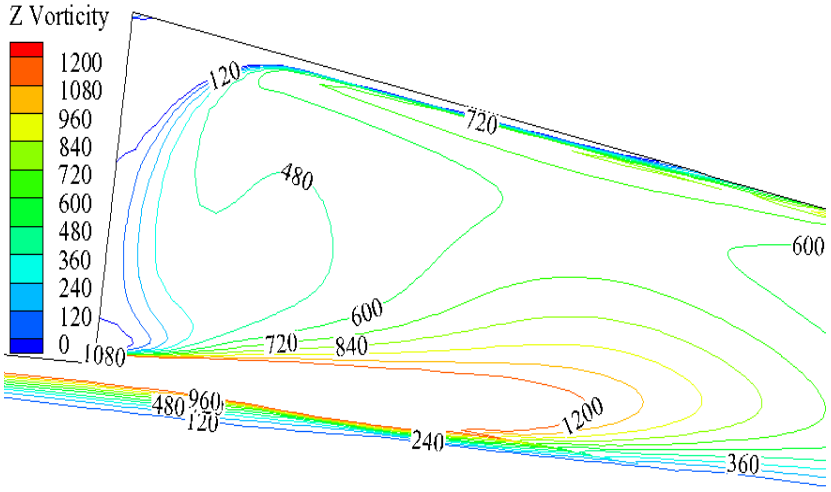

(a).

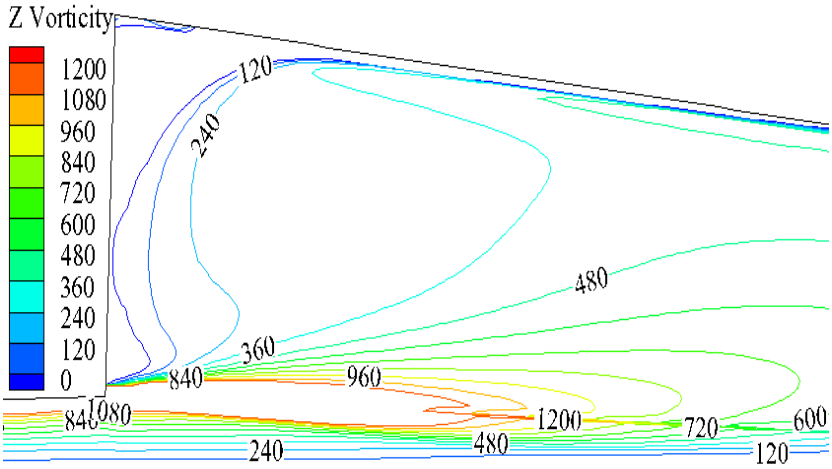

(b).

Figure 3-6: Vorticity Contours in the step cavity of a modified NACA 4415 airfoil; X_l =0.5; L_l =0.5; and D_l =0.5. (a) α = 8°, Re = 2.5 million; (b) α = 2°, Re = 1.7 million

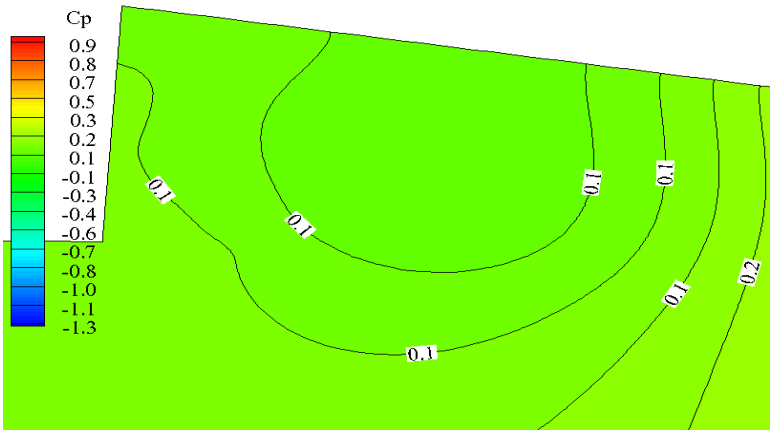

(a).

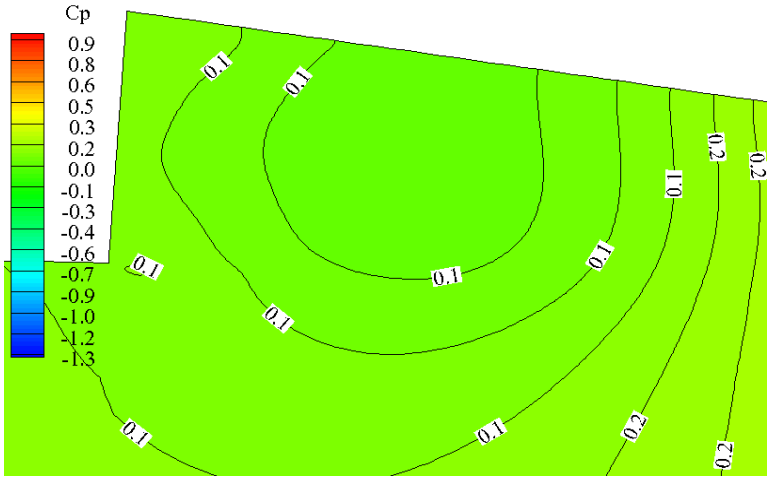

(b).

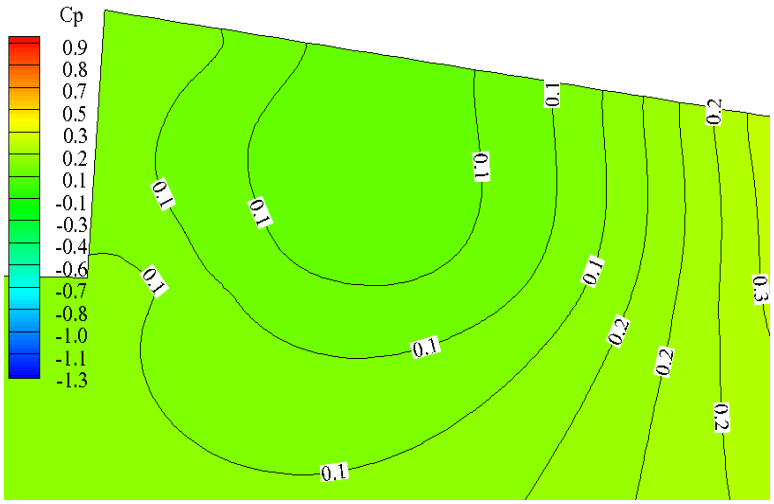

(c).

Figure 3-7: Pressure Contours in the step cavity of a modified NACA 4415 airfoil at $\alpha = 4°$; X_l =0.5; L_l =0.5; and D_l =0.5. (a) Re = 0.6 million; (b) Re = 1.2 million; (c) Re = 1.8 million.

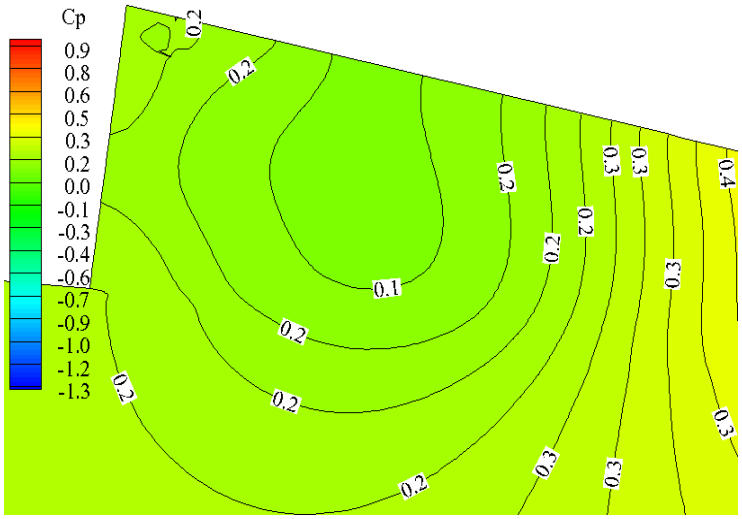

(a).

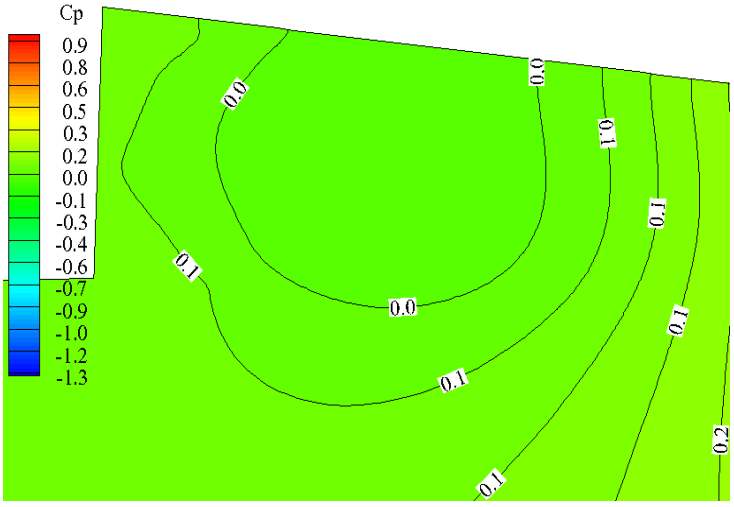

(b).

Figure 3-8: Pressure Contours in the step cavity of a modified NACA 4415 airfoil; X_l =0.5; L_l=0.5; and D_l =0.5. (a) α = 8°, Re = 2.5 million; (b) α = 2°, Re = 1.7 million.

acceleration shown by the Figure 3-1. Further downstream, the pressure builds up till it reaches the undisturbed air pressure level. In contrast to the pressure field on the upper surface, there is not much variation in the pressure on the lower surface except in the step cavity due to the formation of vortices and rettachment of flow downstream. From the plots for stepped configurations in Figure 3-7, it can be seen that with the increase in Re, there is higher change in pressure (ΔP) around the airfoil though the overall trend remains the same for all the cases shown in Figure 3-7. The magnitude of of pressure in the region of flow reattachment in the step cavity is higher at higher angles of attack which can be observed from the pressure plots by comparing Figure 3-7(c) and Figure 3-8 in the for α(s) of 2°, 4°, and 8° and Re(s) of 1.7, 1.8, and 2.5 million respectively, as from the Figure 3-7, it can be seen that Re does not have much effect on the pressure in the region of flow reattachment in proportion with the overall changes in the flow field pressure around the airfoil.

In addition to the pressure contour plots, pressure coefficient plots facilitate further understanding of the pressure variation along the edges of the airfoil configurations. Figure 3-9 illustrates the plots of pressure coefficient versus airfoil chord for a range of Re(s) and $\alpha = 4°$. The upper curve in all the plots indicates the variation of pressure coefficient along the airfoil lower surface and vice versa. As can be noticed from the plots for base airfoil cases in Figure 3-9 and Figure 3-10, the lower surface pressure distribution flattens out after an initial curvy portion which clearly is not the case with the stepped airfoil configurations. The effect of introducing a step is evident from this observation. From the plots for stepped airfoil cases, it is very clear that starting from the step face there is a slight drop in pressure due to the presence of trapped vortices. As we move further downstream, there is an increase in the pressure on the lower surface resulting from the force exerted by the large rotating vortex on the airfoil surface. As can be observed from the plots, the pressure on the airfoil edge comprising the step is higher than that for the base airfoil cases. This observation is consistent for all the stepped airfoil cases. This

explains the higher C_l values and the corresponding lift to drag ratios which will be discussed further in the following section of this thesis.

3.1.1.3. Aerodynamic coefficients. All the aerodynamic characteristics including lift, drag, and moment coefficients directly result from the pressure distributions around the airfoil at a given set of operating conditions. As the present study considers a range of Re(s) and airfoil configurations at different α's, the whole set of flow conditions bring about many cases for study. The plots in Figure 3-11 show the % change in lift coefficient (ΔC_l) for various cases studied at α = 2° without the use of active flow control using jet. ΔC_l here represents the difference in C_l obtained with the unmodified airfoil and the modified airfoil with step. A positive value indicates an increase in C_l and a negative value indicates a decrease in C_l with respect to the unmodified airfoil. Percent change in lift coefficient for any modified airfoil case is defined by

$$\% \text{ change in } C_l = \frac{\Delta C_l}{C_l \text{ for base airfoil}} * 100 \qquad (3.2)$$

Figure 3-12 shows the lift to drag ratio plots obtained from the lift and drag data for α = 2°. Figure 3-13 shows the plots for % change in lift coefficient for cases studied at α = 4° followed by the lift to drag ratio plots shown in Figure 3-14. Figures 3-15 and 3-16 present the corresponding plots for cases studied at α = 8°. Figures 3-11; 3-13; and 3-15 show that ΔC_l obtained with the use of step on the lower surface of a NACA 4414 airfoil is positive for all the cases meaning the stepped airfoil produces higher lift than the base airfoil. It is the highest for the case with Re = 2.5 million, the trend being the same at all α's ranging from about 20% to 35% increase over the base airfoil. In Figure 3-11 the ΔC_l obtained as Re increases from 0.6 million to 1.2 million is higher than that obtained as Re increases from 1.2 million to 1.8 million. Figures 3-12; 3-14; and 3-16 have plots comparing the lift to drag ratio for the base airfoil and stepped

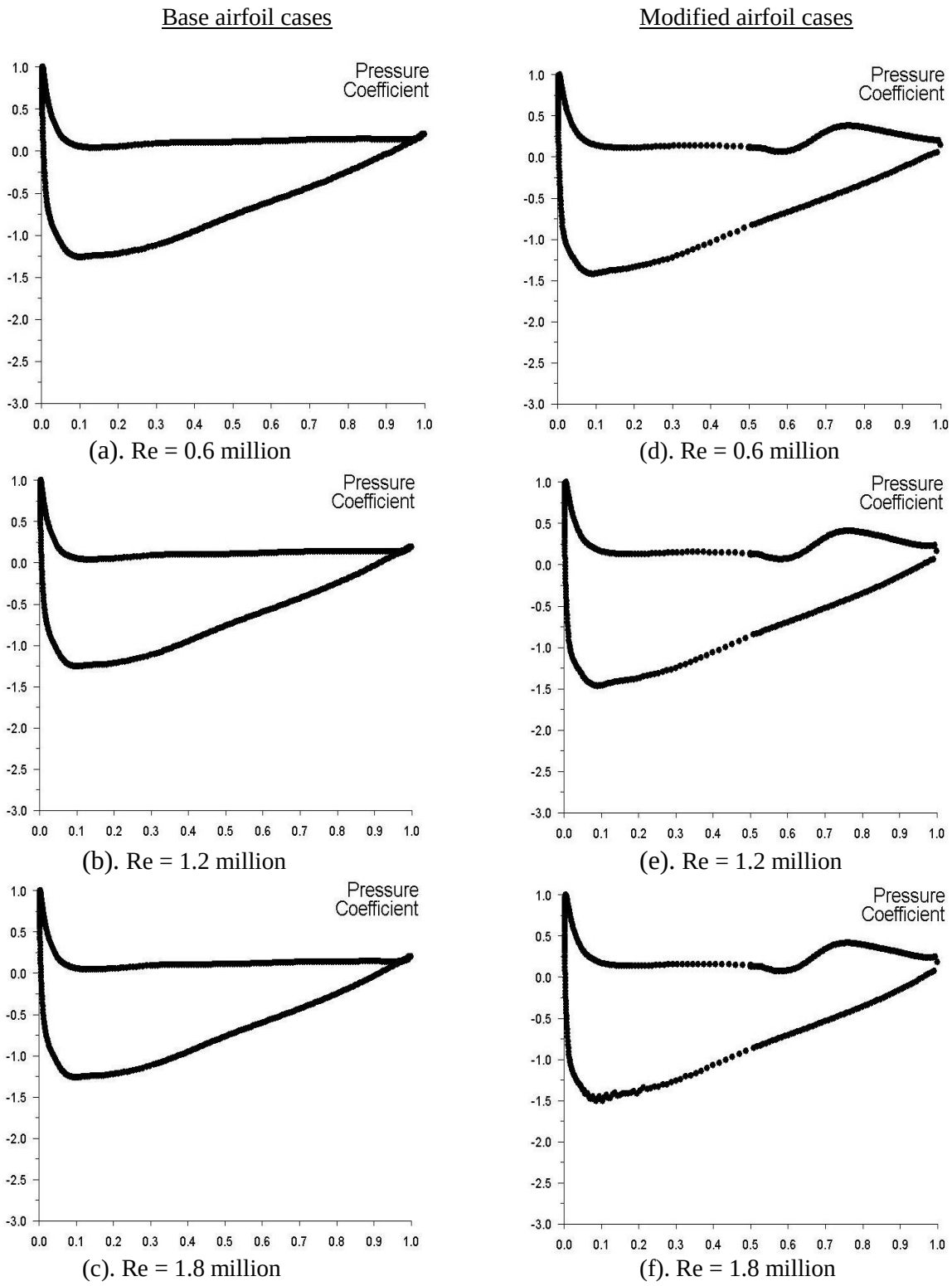

Figure 3-9: Pressure Coefficient versus chord of airfoils at $\alpha = 4°$ for a range of Re(s). Left column: NACA 4415 (base) airfoil; Right column: Modified airfoil with step on the lower surface

Base airfoil cases

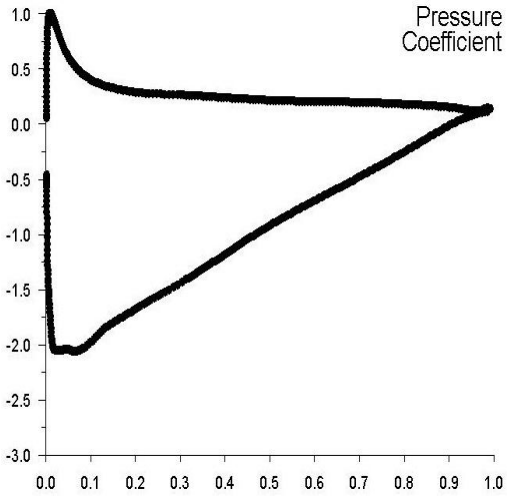

(a). α = 8°; Re = 2.5 million

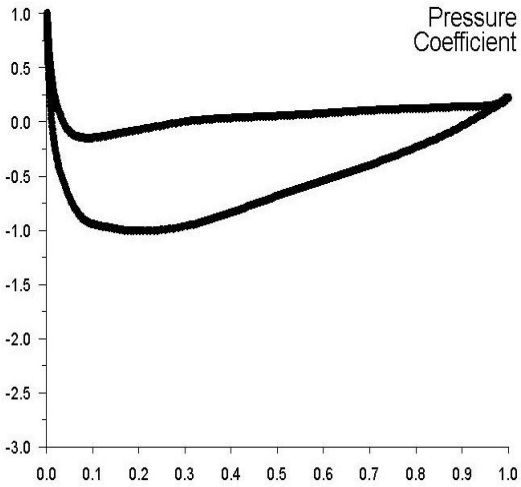

(b). α = 2°; Re = 1.7 million

Modified airfoil cases

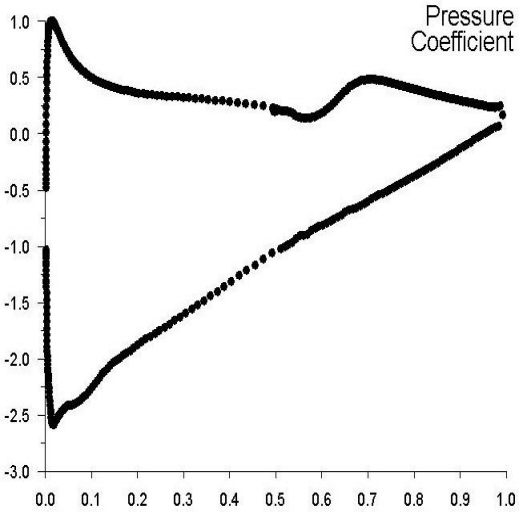

(c). α = 8°; Re = 2.5 million

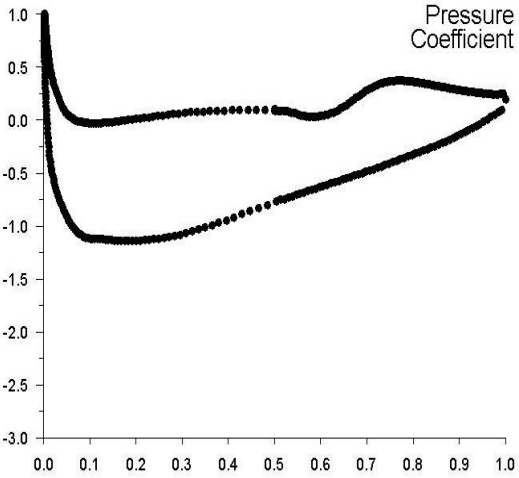

(d). α = 2°; Re = 1.7 million

Figure 3-10: Pressure Coefficient versus chord of airfoils for different α(s) and Re(s). Left column: NACA 4415 (base) airfoil; Right column: Modified airfoil with step on the lower edge.

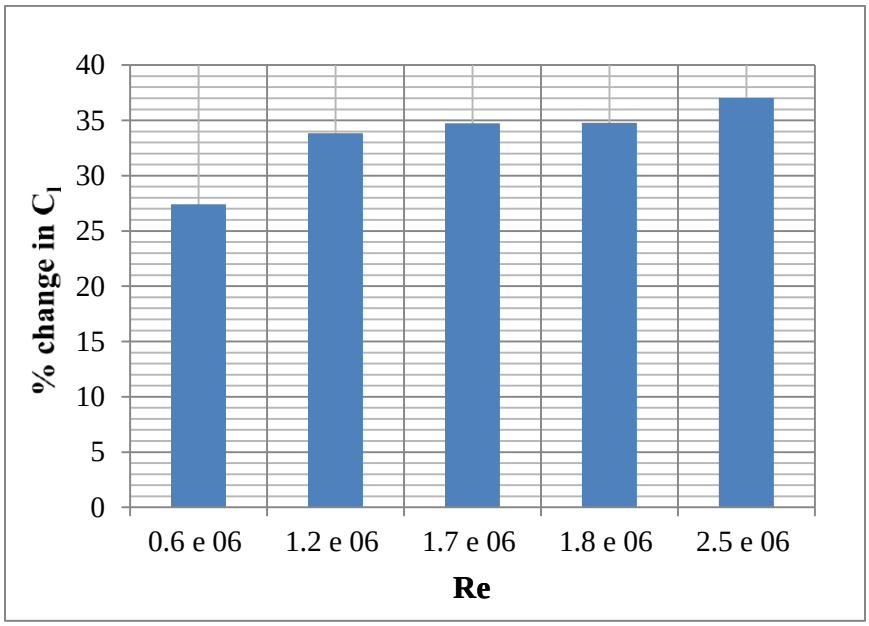

Figure 3-11: Comparison of lift characteristics for modified airfoil configurations for α = 2° and a range of Re(s).

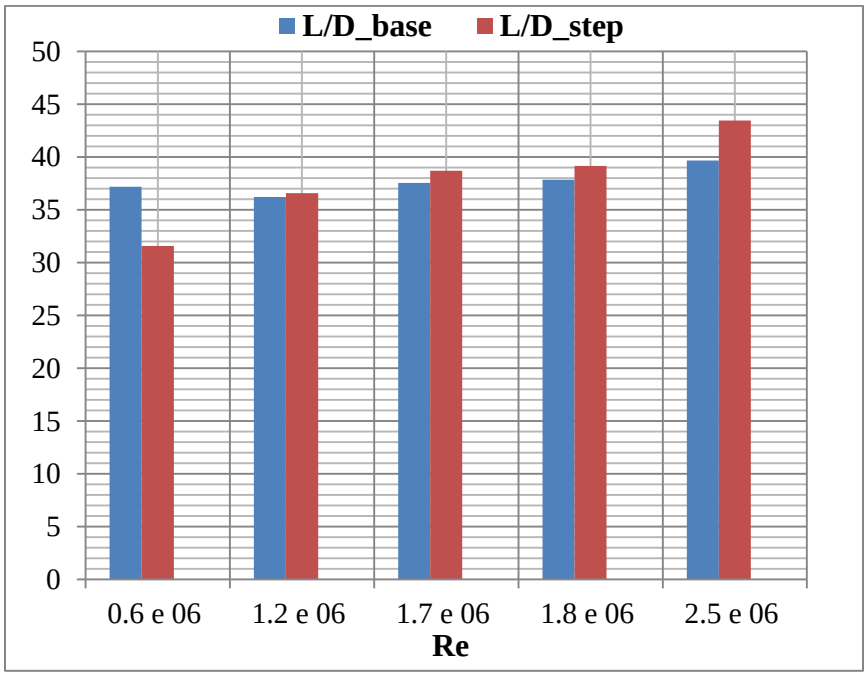

Figure 3-12: Comparison of Lift to Drag Ratio of base and modified airfoil configurations for α = 2° and a range of Re(s).

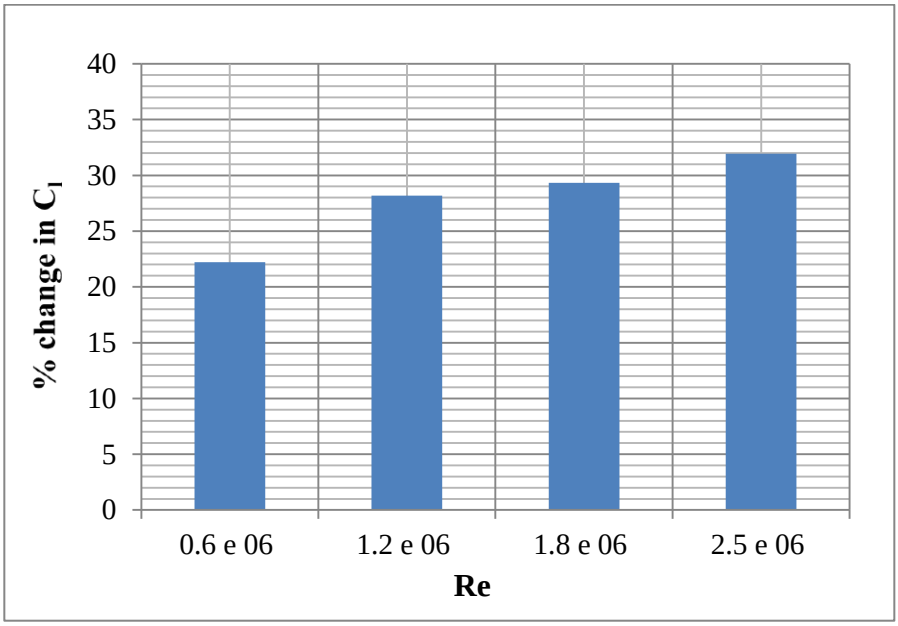

Figure 3-13: Comparison of lift characteristics for modified airfoil configurations for α = 4° and a range of Re(s).

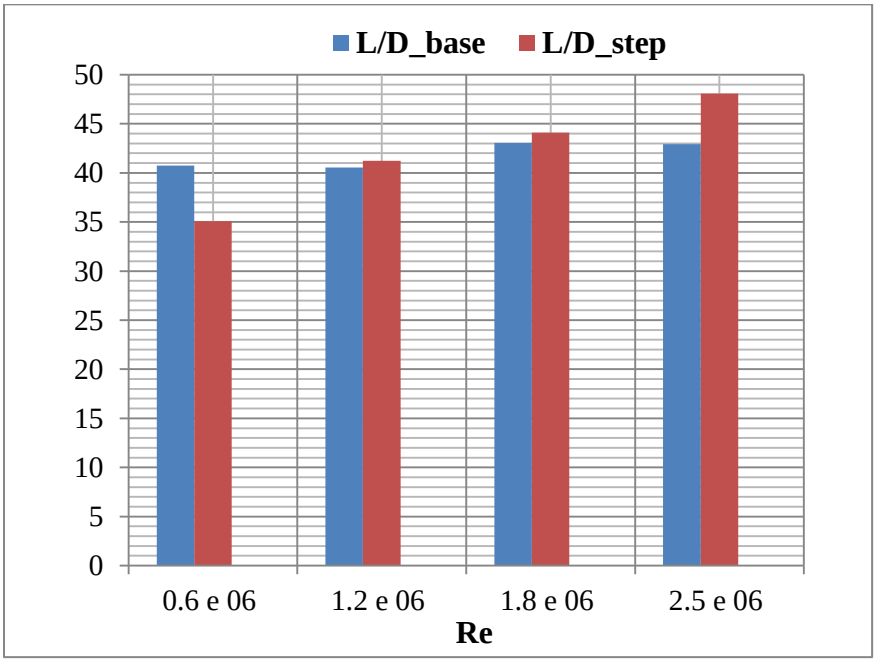

Figure 3-14: Comparison of Lift to Drag Ratio of base and modified airfoil configurations for α = 4° and a range of Re(s).S

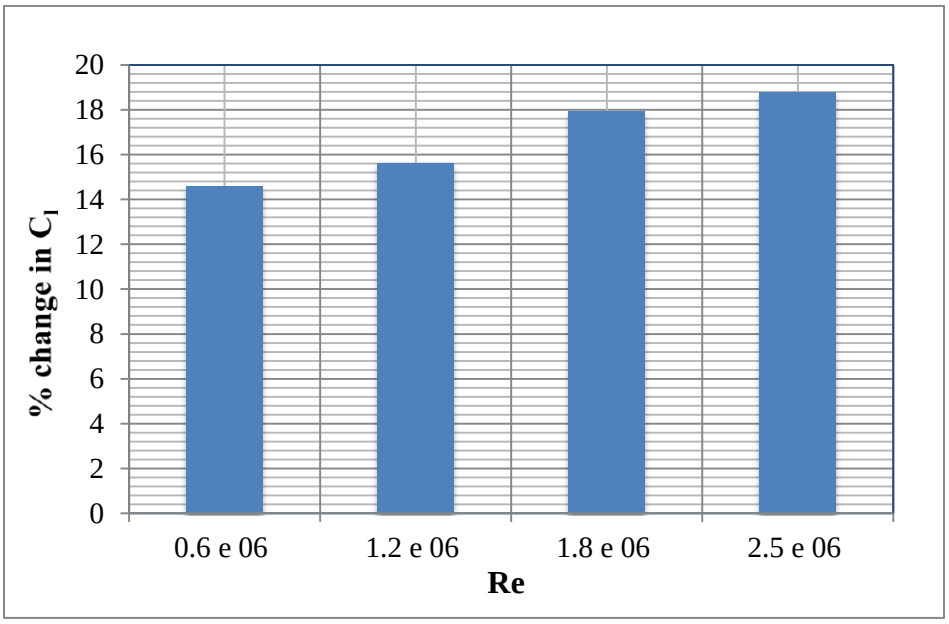

Figure 3-15: Comparison of lift characteristics for modified airfoil configurations for α = 8° and a range of Re(s).

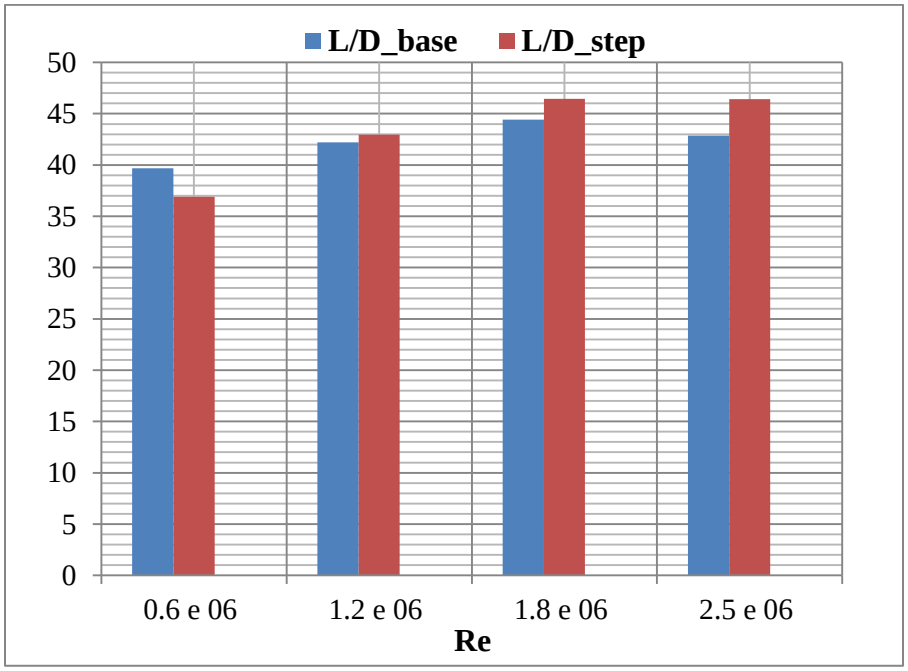

Figure 3-16: Comparison of Lift to Drag Ratio of base and modified airfoil configurations for α = 8° and a range of Re(s).

airfoil for the various cases studied. This trend with the L/D ratios for the stepped airfoils is also noticeable in the plots shown in these figures. The values of L/D ratio are higher for the stepped airfoil cases than those of the base airfoil cases for all Re's except for Re = 0.6 million. Though there is an increase in C_l over the base airfoil cases for all the stepped airfoil cases, there is rise in C_d as a consequence of the use of step. The contributions to the higher lift to drag ratios come from the significant increments in C_l for the modified airfoil cases.

3.1.2. Active Flow Control Using Jet. The previous section dealt with all the cases studied without the use of jet or external energy for flow control. This section deals with the use of air injecting jets to alter the flow field by controlling the trapped vortex in order to enhance the aerodynamic performance of stepped airfoils which parallels with the title of this thesis. Thus this section was titled as such. The effect of using an air injecting jet in the step cavity was studied on a NACA 4415 airfoil with a backward facing flat step introduced on the lower surface.

3.1.2.1. Influence of air injecting jet placed in the step cavity. This study focuses on understanding the effect of an air injecting jet placed in the step cavities on the aerodynamic characteristics of stepped airfoils with an objective of enhancing their aerodynamic performance. The cases were studied with the jets placed at two different locations and the jet is injected at four different angles 0°, 15°, 30°, and 45° made with the direction of free stream velocity which coincides with the X-axis respectively from each location as shown in Figure 3-17 thus forming several cases for study. Figure 3-17 shows the locations of the jets placed on the top and bottom of the step. Table 3-2 enlists all the cases studied using a jet as a part of this research. In all the cases discussed in this section, the passive flow control technique realized as a step created on the lower side of a NACA 4415 airfoil is augmented by the use of external energy in the form of an air injecting jet to control the flow field within the step cavity.

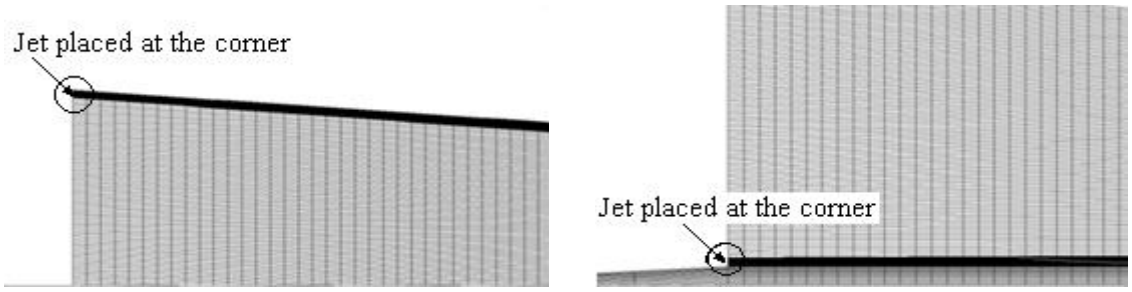

(a). (b).

Figure 3-17: Jet placed in the step cavity at different locations. (a) on the top; (b) on the bottom

Table 3-2: Summary of modified NACA 4415 airfoil cases studied using jet in the step cavity at $\alpha = 2°$; Re = 1.7 million.

Case No.	Jet Parameter		
	ζ	$C\mu$	V_j / U_∞
17	0°	0.00027	0.25
18	0°	0.00108	0.5
19	0°	0.00243	0.75
20	0°	0.00433	1.0
21	0°	0.00974	1.5
22	0°	0.01731	2.0
23	15°	0.00027	0.25
24	15°	0.00108	0.5
25	15°	0.00243	0.75
26	15°	0.00433	1.0
27	15°	0.00974	1.5
28	15°	0.01731	2.0
29	30°	0.00027	0.25
30	30°	0.00108	0.5
31	30°	0.00243	0.75
32	30°	0.00433	1.0
33	30°	0.00974	1.5
34	30°	0.01731	2.0
35	45°	0.00027	0.25
36	45°	0.00108	0.5
37	45°	0.00243	0.75
38	45°	0.00433	1.0
39	45°	0.00974	1.5
40	45°	0.01731	2.0

The mass flow rate of injection corresponds to the jet velocity (V_j) set for each case studied. The other parameter used for characterizing the jet is the angle of the jet (ζ). The width of the jet is about 3.22% of the depth of the step. Since the free-stream density and width of the jet are fixed, the mass flow rate is a direct function of V_j. When the jet velocity takes the value equal to the free-stream velocity of 24.93 m/s, the mass flow rate is about 0.07 kg/s. Use of jets in the step cavities produced interesting results. Preliminary results obtained for cases with jet placed at each location and for different angles of injection show that jet placed on the bottom of the step face produces the best results overall with regard to the aerodynamic characteristics. Kitsios[21] et al through their research involving numerical study of NACA 0015 airfoil using Zero Net Mass Flux (ZNMF) jets concluded that jets placed closer to the uncontrolled separation point require a lower jet velocity to achieve the desired lift enhancement. In other words, for a given jet velocity, higher lift coefficient is obtained when the jet is placed closer to the separation point. In the present study, it was observed that the jet placed at the corner of the step where the flow separates from the edge / surface of the airfoil which proves the observation made by them. Thus further investigation was conducted by placing the jet on the step bottom. Another observation made by the same research group mentioned above is that spreading rates of the jet effluxes and decay constants of oscillatory jets were higher than those of continuous jets in case of circular jet orifices. However, the current study involves a preliminary step in the studies on application of active flow control on stepped airfoils. Hence continuous jets are chosen for the entire study. All the results for the cases with jet were obtained for fixed inlet conditions of $\alpha = 2°$ and Re = 1.7 million. Since this particular flight attitude condition corresponds to the cruise regime of the UAV Pioneer considered for the case study discussed later in this thesis, the focus in this investigation with regard to the enhancement of aerodynamic performance of stepped airfoils using jets was kept on the modified airfoil cases at $\alpha = 2°$ with the Reynolds number fixed at 1.7 million and the corresponding U_∞ at 24.93 m/s. Figure 3-18 illustrates the various jet and step

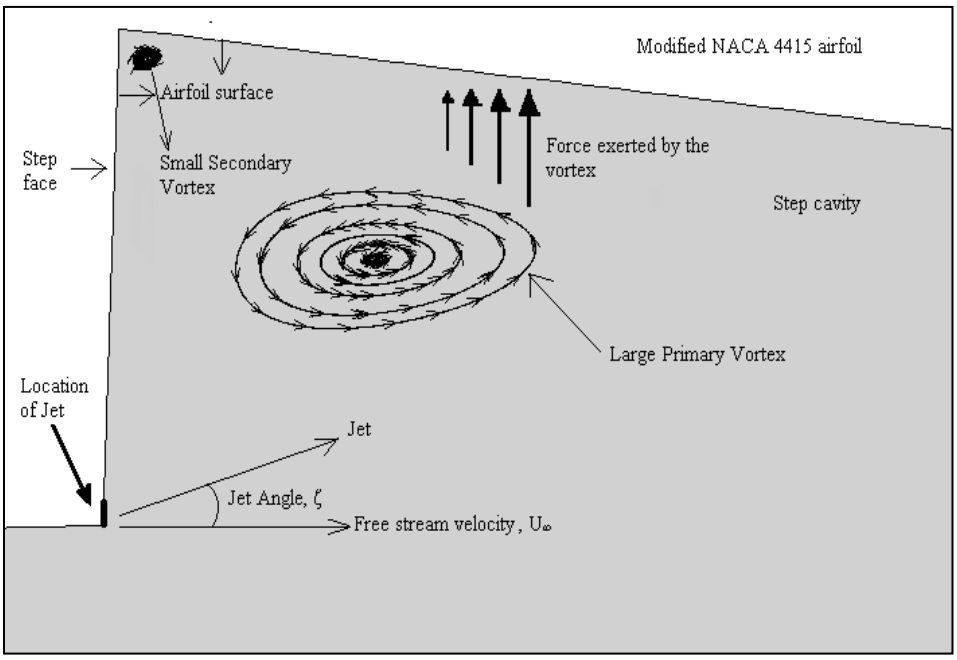

Figure 3-18: Illustration depicting the influence of jet on the stepped airfoil.

geometry parameters along with the key flow developments in the step cavity of a modified airfoil using jet. As can be seen the vortex system existing within the step cavity comprises the large, primary vortices rotating counter-clockwise and the small, counter-rotating, secondary vortices. There are three main observed effects of jet on the flow field characteristics. First, the noticeable effect of jet is the pinching of the vortex system. It can be observed in all the jet cases that the jet is squeezing the large primary vortex. This can be easily realized by comparing the velocity contour and streamline plots presented in the next section for the modified airfoil cases without jet with those for the jet cases in the Figures 3-3, 3-4, and the plots for the jet cases discussed in the next section. Table 3-3 quantifies the dependence of the location of the center of vortex formed in the step cavity on the jet angle by comparing the jet cases with those of the stepped airfoil without a jet. The degree of the squeeze increases with the increase in the angle of the jet placed within the step cavity. Secondly, the effect of the jet is to result in an increase in the lift due to the increased force exerted by the vortex as illustrated in Figure 3-18. This increase in

Table 3-3: The effect of ζ on the location of center of vortex with Cμ fixed at 0.01731; $V_j = 2U_\infty$.

Jet Angle, ζ	Distance of the votex center from the step face / step length
step without jet	0.180
0°	0.110
15°	0.105
30°	0.100
45°	0.090

the force exerted upon the airfoil surface by the vortex is because of the introduction of jet in which case the vortex system is strengthened with regions of acceleration visible in the outer layers of the large primary vortex in the flow visualization plots which will be discussed further in the next section. The third effect of the jet could be explained using the basic principles of action and reaction. Reflecting on the fundamental concept of a jet flap[18] to better understand the influence of jet on the flow field characteristics, a jet flap is a thin, high energy jet that is directed downward at some angle with respect to the free stream. The effect of the jet flap is to creat a reaction force / lift due to the vertical component of the jet momentum. With a slight modification in the purpose of jet which in this research is to influence the flow field and attempt to control the trapped vortices in the step cavity, the effect of the jet could possibly be understood as one which generates a reaction force that acts in the direction opposite to the drag thus canceling part of the drag force acting on the airfoil. The result is reduced drag which is evident from the plots showing the dependence of the aerodynamic characteristics of stepped airfoil on the jet parameters of ζ and V_j. The results will be discussed in detail in the Section 3.1.2.4 of this thesis.

3.1.2.2. Velocity contours and streamlines. Figure 3-19 illustrates the flow field as streamlines superimposed on velocity contours colored by velocity magnitude over a

modified NACA 4415 airfoil with a step using a jet placed in the step cavity as shown in the Figure 3-17(b). Figure 3-20 presents the pressure contours for the same case. The velocity contours in Figure 3-19 are colored by dimensionless velocity v as defined in the Section 3.1.1.1. The dimensionless velocity ranges from 0 to 2 in steps of 0.25 as shown by the legend. This case of study is same as that of the case for $\alpha = 2°$, Re = 1.7 million discussed earlier in this chapter in addition to which active flow control realized using a jet was employed for enhancing the aerodynamic performance. The jet is ejected at angle of 45° with a jet coefficient $C\mu = 0.01731$ corresponding to jet velocity $V_j = 2U_\infty$. The effect of jet is to energize the flow field within the step cavity which is more obvious from the Figure 3-21. In the figure, regions of acceleration can be spotted in the outer layers of the vortex in all of the three jet cases. From the figures, it is evident that the jet has an identifiable effect on the flow field by accelerating the flow within the vortex system. In other words, the jet is energizing the flow thereby strengthening the vortex. The pinching nature of the jet along with the flow acceleration caused by the jet in the step cavity act together to strengthen the vortex system prevalent in the step cavity. This explains and is evident from the benefits in terms of the lift and drag characteristics obtained from the use of jet at different angles over the modified airfoil with a step without jet which will be discussed in detail in the following sections. From the vorticity contours shown in Figure 3-22, it can be observed that there is a slight variation in the vorticity distribution within the step cavity when $C\mu$ is varied keeping ζ fixed. The vorticity gradients increase as the jet velocity is varied which can be understood by comparing the plots in Figures 3-22 and 3-23.

3.1.2.3. Pressure distributions. Plots illustrating the pressure distributions facilitate better understanding of the various flow developments associated with the use of jet placed in the step cavity. Figure 3-20 presents the global view of pressure distribution around the modified NACA 4415 airfoil at $\alpha = 2°$, and Re = 1.7 million with a step using a jet placed in the

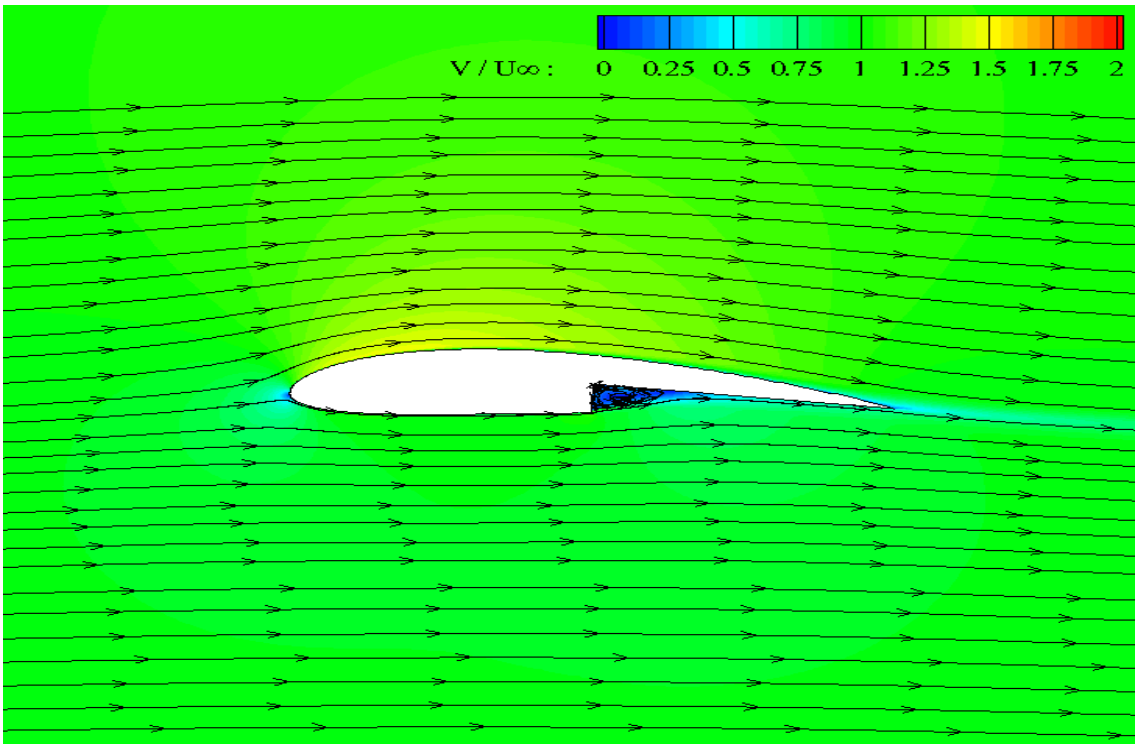

Figure 3-19: Global View of Velocity Contours and Streamlines around a stepped NACA 4415 airfoil using a jet placed in the step cavity with jet parameters $\zeta = 45°$, $C\mu = 0.01731$ at $\alpha = 2°$; Re = 1.7 million; $X_l = 0.5$; $L_l = 0.5$; and $D_l = 0.5$.

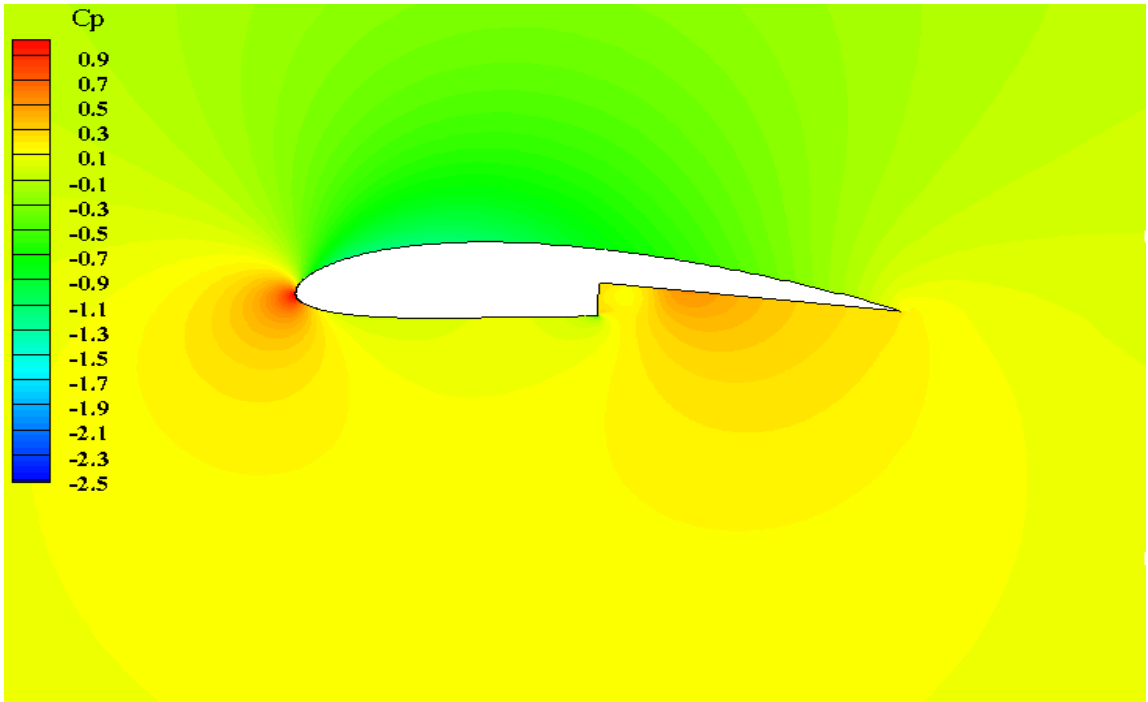

Figure 3-20: Global View of Pressure Contours around a stepped NACA 4415 airfoil using a jet placed in the step cavity with jet parameters $\zeta = 45°$, $C\mu = 0.01731$ at $\alpha = 2°$; Re = 1.7 million; $X_l = 0.5$; $L_l = 0.5$; and $D_l = 0.5$.

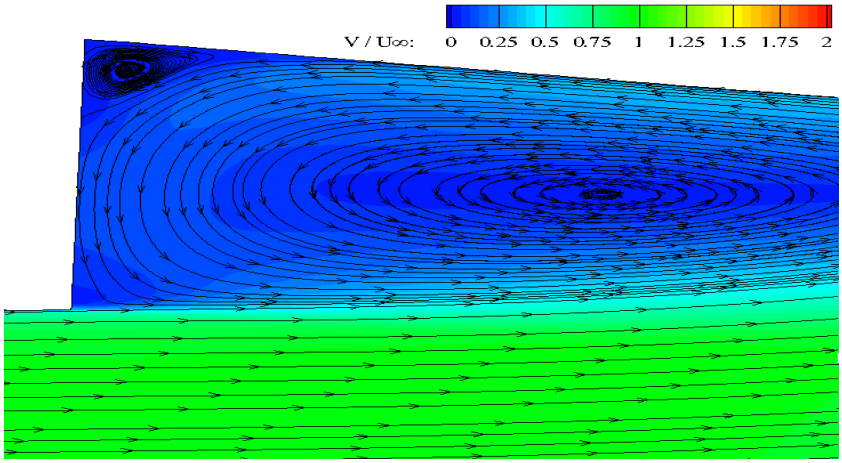

(a).

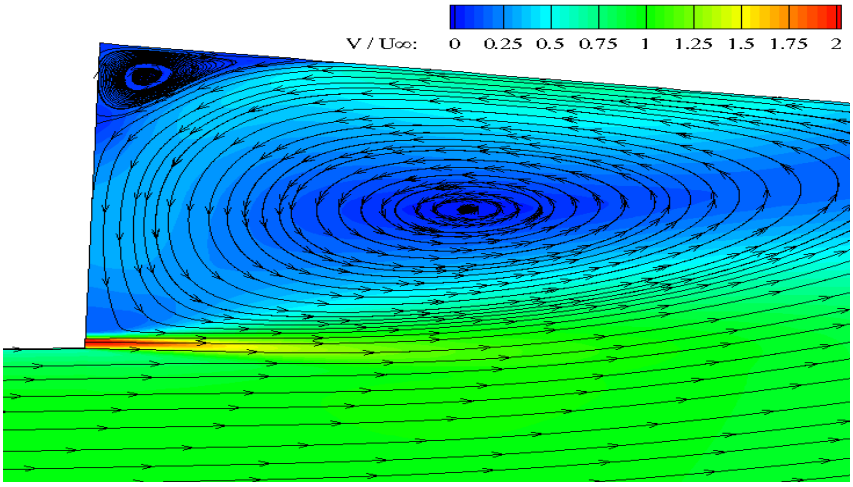

(b).

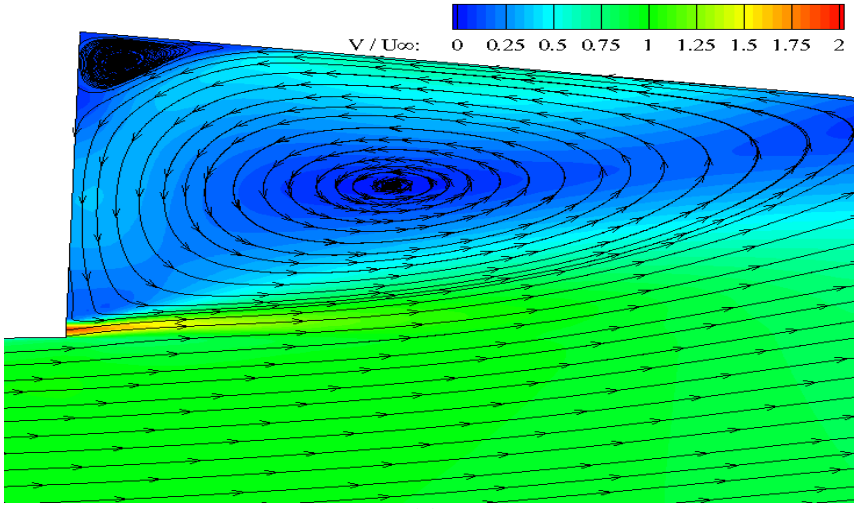

(c).

Figure 3-21: Velocity Contours and Streamlines in the step cavity of a modified NACA 4415 airfoil using a jet placed in the step cavity with jet parameter $C\mu = 0.01731$ at $\alpha = 2°$, Re = 1.7 million; $X_l = 0.5$; $L_l = 0.5$; and $D_l = 0.5$. (a) step without jet; (b) $\zeta = 0°$; (c) $\zeta = 15°$

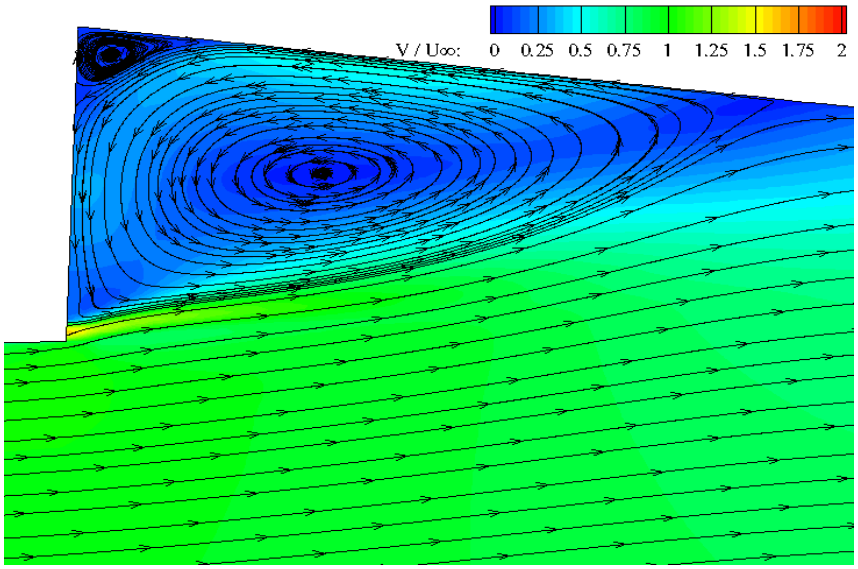

(d).

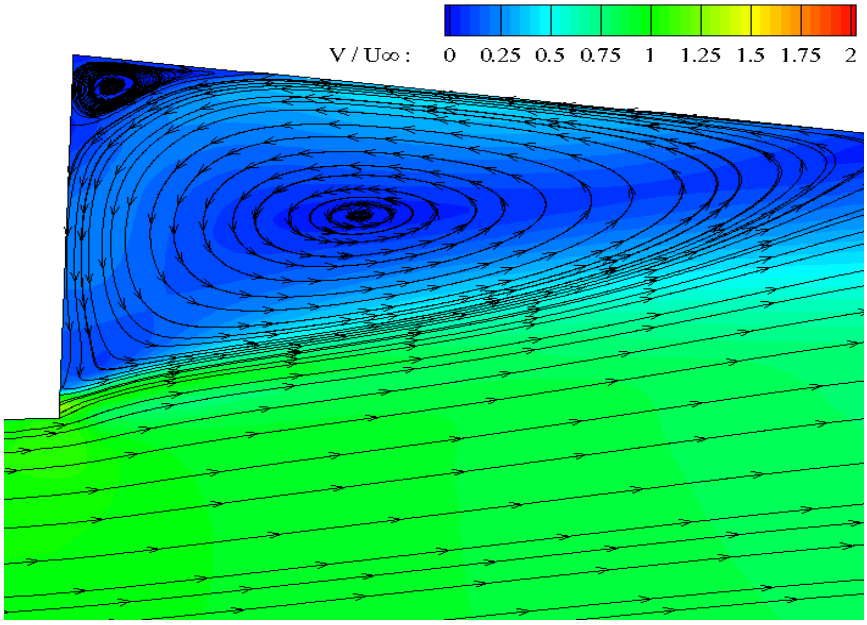

(e).

Figure 3-21: Velocity Contours and Streamlines in the step cavity of a modified NACA 4415 airfoil using a jet placed in the step cavity with jet parameter $C\mu = 0.01731$ at $\alpha = 2°$, Re = 1.7 million; $X_l = 0.5$; $L_l = 0.5$; and $D_l = 0.5$. (contd.) (d) $\zeta = 30°$; (e) $\zeta = 45°$

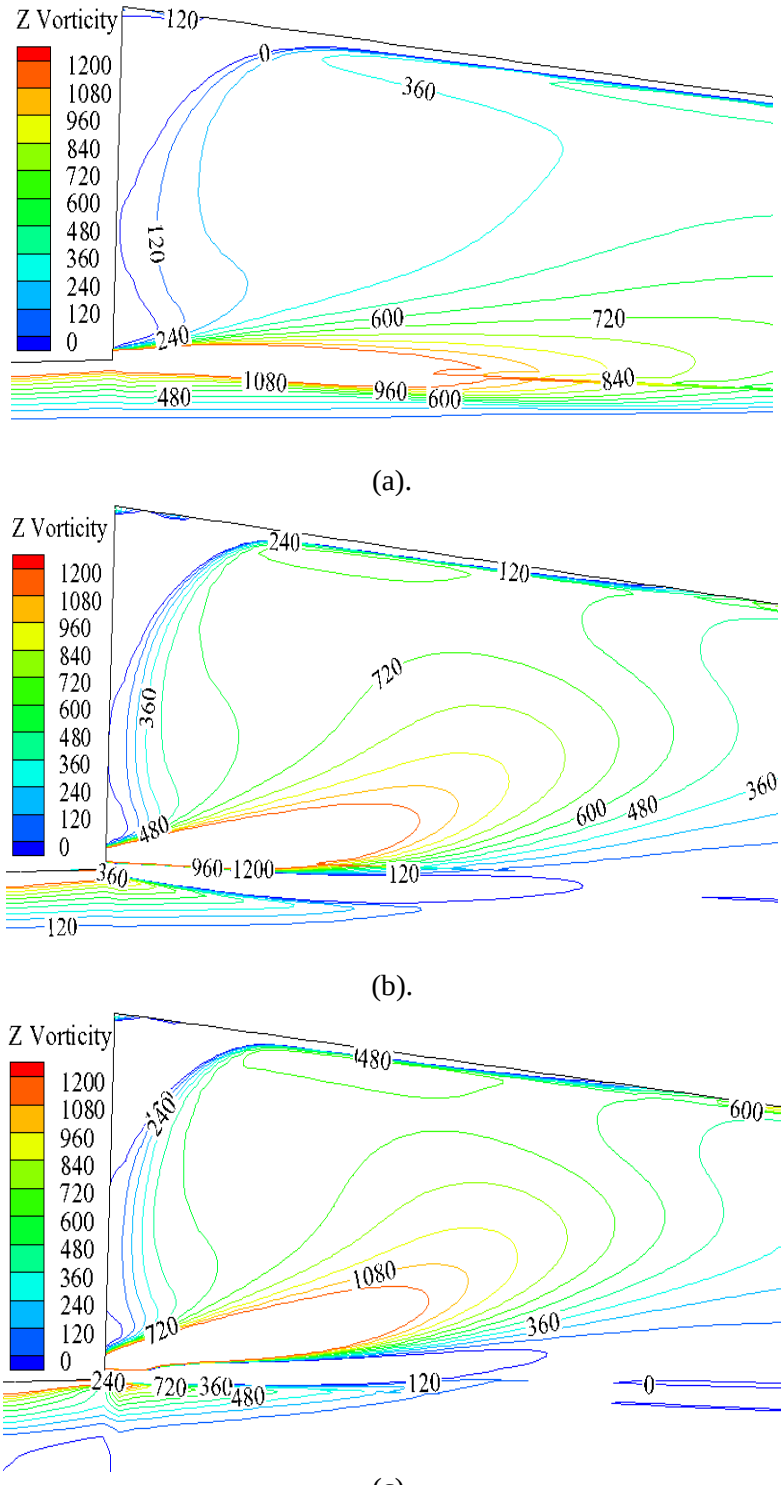

Figure 3-22: Vorticity Contours in the step cavity of a modified NACA 4415 airfoil using a jet placed in the step cavity with jet parameter Cμ = 0.01731 at α = 2°, Re = 1.7 million; X_l =0.5; L_l =0.5; and D_l =0.5. (a) step without jet; (b) ζ = 0°; (c) ζ = 15°

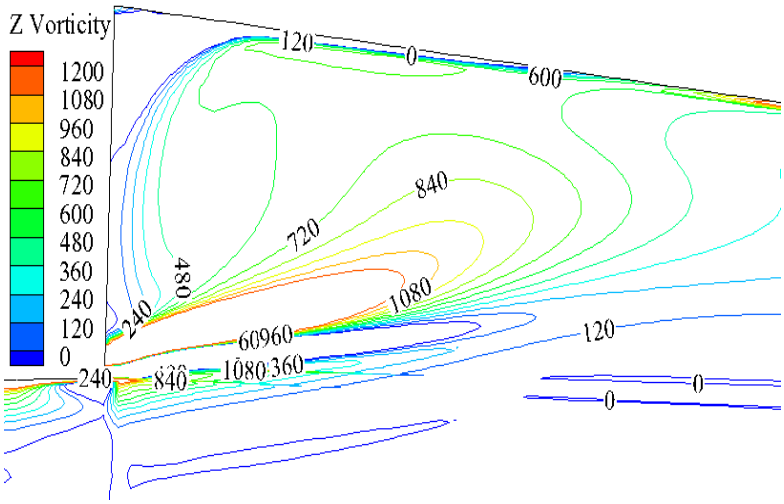

(d).

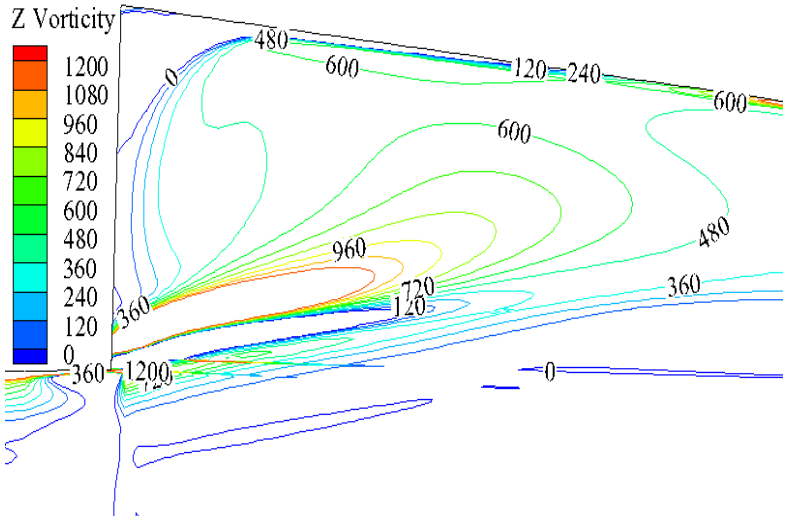

(e).

Figure 3-22: Vorticity Contours in the step cavity of a modified NACA 4415 airfoil using a jet placed in the step cavity with jet parameter Cμ = 0.01731 at α = 2°, Re = 1.7 million; X_l =0.5; L_l =0.5; and D_l =0.5. (contd.) (d) ζ = 30°; (e) ζ = 45

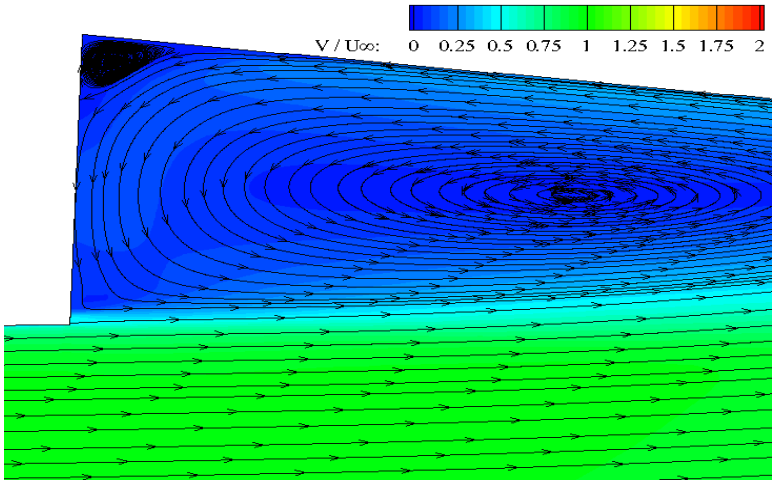

(a).

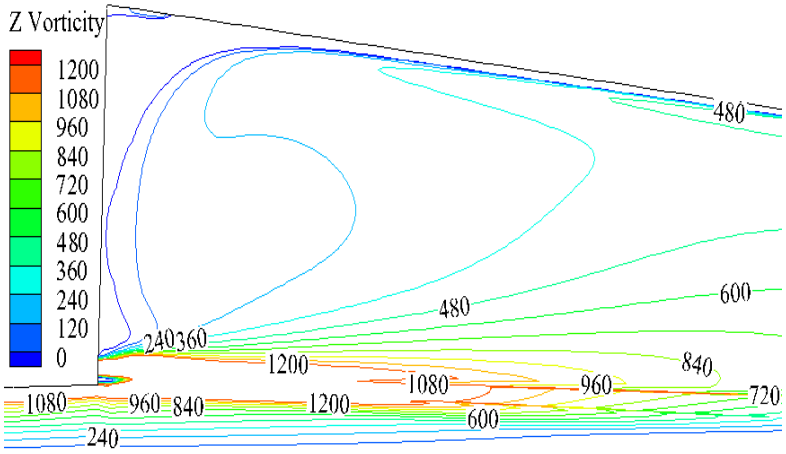

(b).

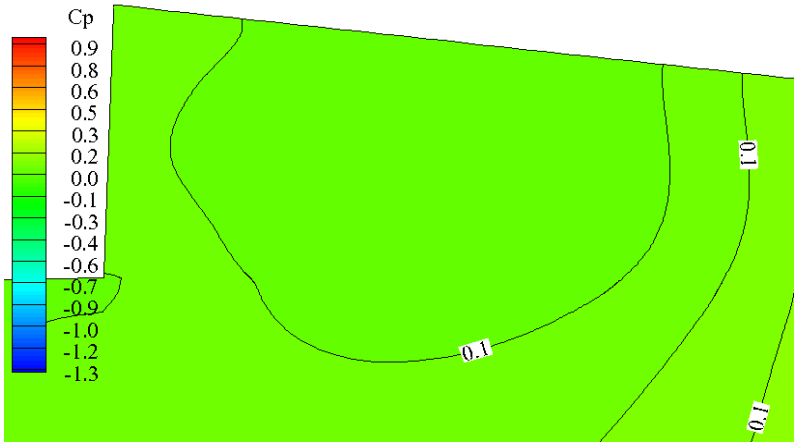

(c).

Figure 3-23: Flow field within the step cavity of a modified NACA 4415 airfoil using a jet placed in the step cavity with jet parameters $\zeta = 15°$; $C\mu = 0.00108$ at $\alpha = 2°$, Re = 1.7 million; $X_l = 0.5$; $L_l = 0.5$; and $D_l = 0.5$. (a) Velocity Contours and Streamlines; (b) Vorticity Contours; (c) Pressure Contours

step cavity. The jet parameters are $\zeta = 45°$, and $C\mu = 0.01731$ corresponding to $V_j = 2U_\infty$. The contours in the plot showing the global pressure distribution are colored by the magnitude of pressure coefficient which ranges from -2.5 to 1. From the figure, it can be seen that there is flow stagnation in front of the airfoil. The pressure increases on the bottom surface as the flow progresses while on the top surface it decreases. As can be observed from the plot, there is higher variation in the pressure on the upper surface than that on lower surface. The pressure takes the highest values in the stagnation region around the airfoil leading edge while the lowest values occur on the upper surface. Figure 3-24 illustrates the magnified pressure contour plots showing the variation in pressure within the region of the step cavity. The C_p on the legend varies from -1.3 to 1 on all these plots. Comparing the case of stepped airfoil using jet at $\zeta = 0°$ with that of the modified airfoil case without jet shown in Figure 3-24(a), there is a slight variation in the pressure due to the introduction of jet. There is a substantial increase in pressure as ζ is increased to 30° and further increased to 45°. Pressure gradients are high in the region where the large vortex is stationed and also in the vicinity of the jet indicated by the presence of many pressure contours spaced closer. In all the C_p plots it can be noticed that the minimum pressure in the step cavity occurs at the vortex core thereby proving the fact that a vortex exhibits a pressure minimum at the center. As compared with the case of stepped airfoil without jet, there is significant variation in the pressure in the step cavities in the jet cases studied due to the influence of jet on the flow field comprising the system of contra-rotating vortices.

Figure 3-25 shows the pressure coefficient plots illustrating the pressure distribution on the airfoil surface for the base airfoil, stepped airfoil, and stepped airfoil with jet cases for $\alpha = 2°$; Re = 1.7 million. As can be seen from Figure 3-25(a) for base airfoil, the lower surface pressure distribution indicated by the lower curve is smooth with not much variation when compared with the plots for various cases. From the plot for stepped airfoil without jet, it is very clear that starting from the step face there is an increase in the pressure on the lower surface. This increase

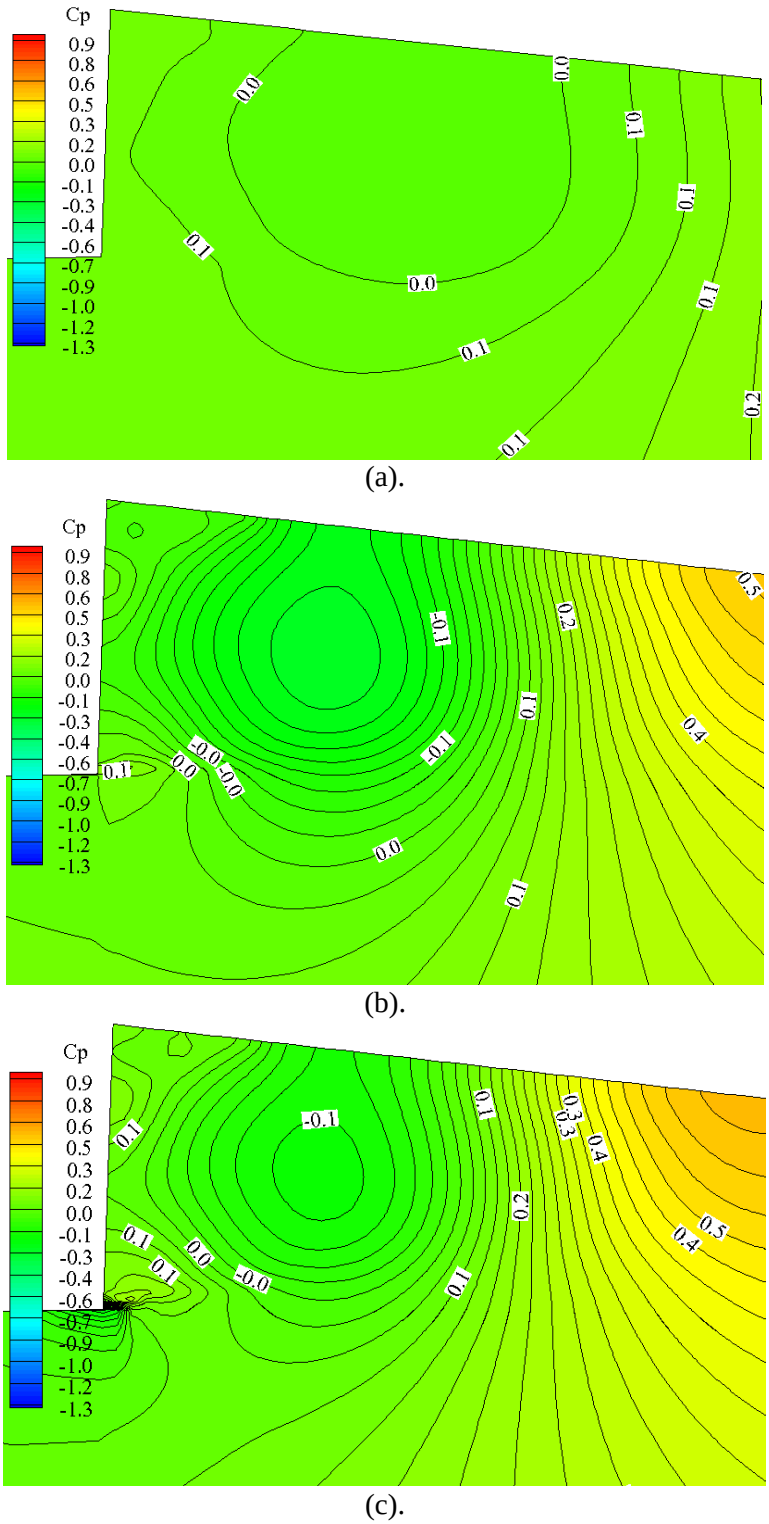

Figure 3-24: Pressure Contours in the step cavity of a modified NACA 4415 airfoil using a jet placed in the step cavity with jet parameter $C\mu = 0.01731$ at $\alpha = 2°$, Re = 1.7 million; $X_l = 0.5$; $L_l = 0.5$; and $D_l = 0.5$. (a) step without jet; (b) $\zeta = 0°$; (c) $\zeta = 15°$

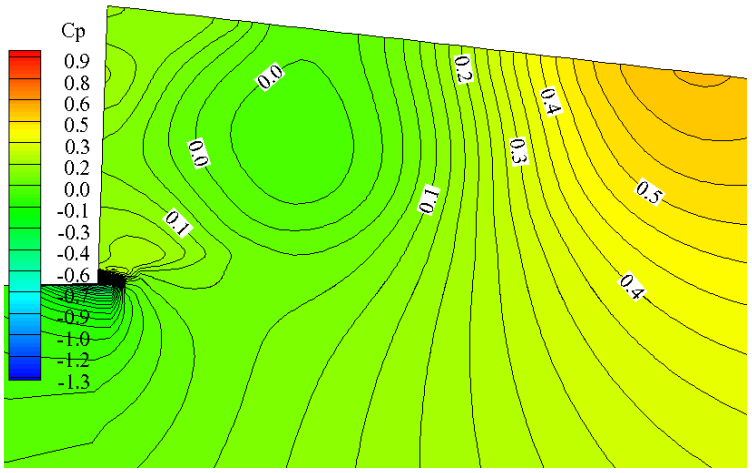

(d).

.

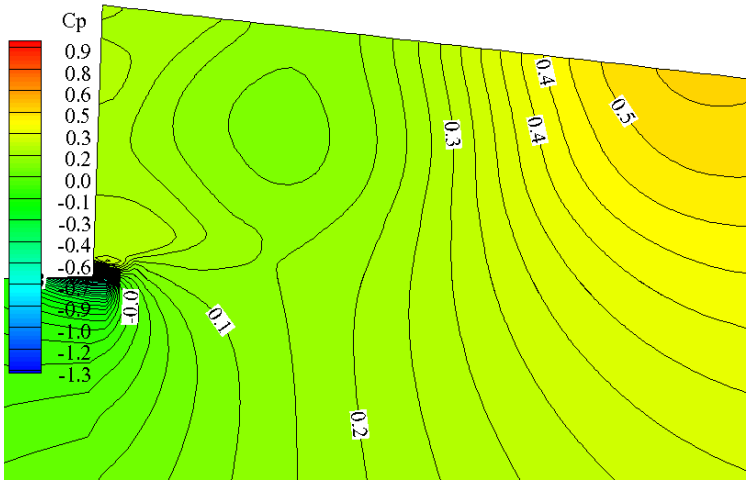

(e).

Figure 3-24: Pressure Contours in the step cavity of a modified NACA 4415 airfoil using a jet placed in the step cavity with jet parameter $C\mu = 0.01731$ at $\alpha = 2°$, Re = 1.7 million; $X_l = 0.5$; $L_l = 0.5$; and $D_l = 0.5$. (contd.) (d) $\zeta = 30°$; (e) $\zeta = 45°$

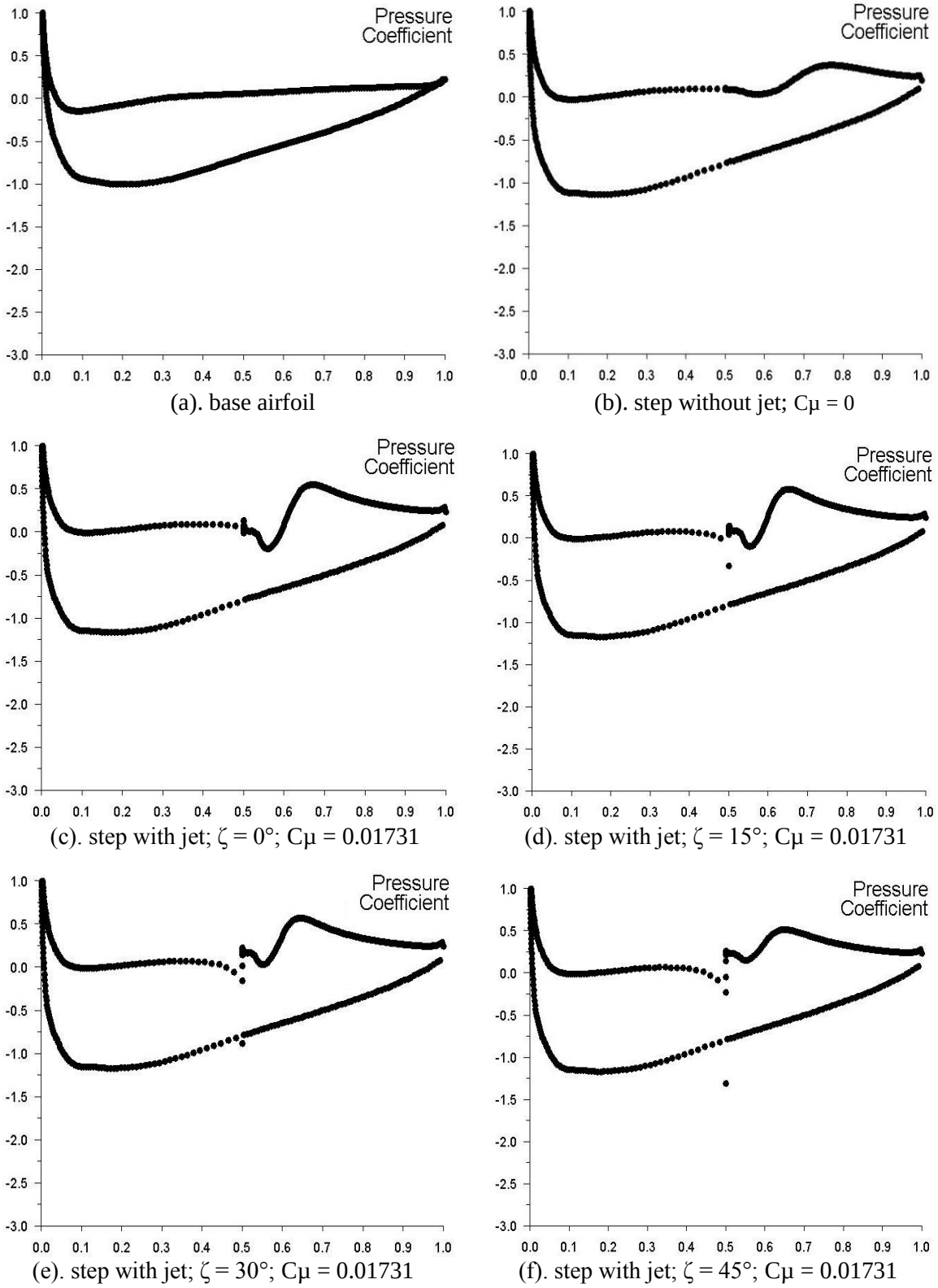

(a). base airfoil

(b). step without jet; Cμ = 0

(c). step with jet; ζ = 0°; Cμ = 0.01731

(d). step with jet; ζ = 15°; Cμ = 0.01731

(e). step with jet; ζ = 30°; Cμ = 0.01731

(f). step with jet; ζ = 45°; Cμ = 0.01731

Figure 3-25: Pressure Coefficient versus chord of NACA 4415 airfoil configurations at α = 2°; Re = 1.7 million for various jet parameters.

in pressure results from the force exerted by the vortex on the wall of the airfoil. This explains the increase in C_l due to the introduction of a step on the lower surface. Figures 3-25(c), (d), (e), and (f) show the pressure coefficient plots for the cases with jet for different jet parameters as mentioned below each plot. The plots for all the cases of step with jet show that the upper surface suction peak is unaltered as shown by the lower curves on the plots though there is much variation in the pressure on the lower surface as shown by the wavy upper curves depicting the distribution of pressure. There is a significant change in the lower surface pressure distribution as compared to the case of step without jet. The sudden drop in the pressure at the step face in all the jet cases is due to the presence of jet itself as the flow velocities are high in the vicinity of the jet. The pressure rises back to normal just past the step face. Moving a little further along the airfoil wall there is a drop in pressure at the point on the wall corresponding to the location of the vortex core directly beneath it. This feature is noticeable in all the jet cases. Moving further downstream, there is a significant rise in the wall pressure due to the force exerted by the vortex on the airfoil surface. This variation in the pressure again, can be observed in all the jet cases. The pressure on the airfoil edge comprising the step in all the jet cases is appreciably higher than that for the stepped case evident from the plots in Figure 3-25. This pronounced variation in the lower surface pressure explains the higher values of C_l obtained for all the jet cases and the corresponding values of L/D ratio which are discussed in detail in the following section.

3.1.2.4. Aerodynamic coefficients. All the information gathered in terms of the lift, drag and moment characteristics results from the pressure distributions discussed earlier in this thesis. Figure 3-26 has three plots showing the lift, drag and lift to drag data generated for the various cases of stepped airfoil using jet along with the case of step without jet. Looking at the figure at a glance to get the broader picture of the influence of jet on the aerodynamic performance of the stepped airfoil, it is evident that use of jet produces benefits by enhancing the

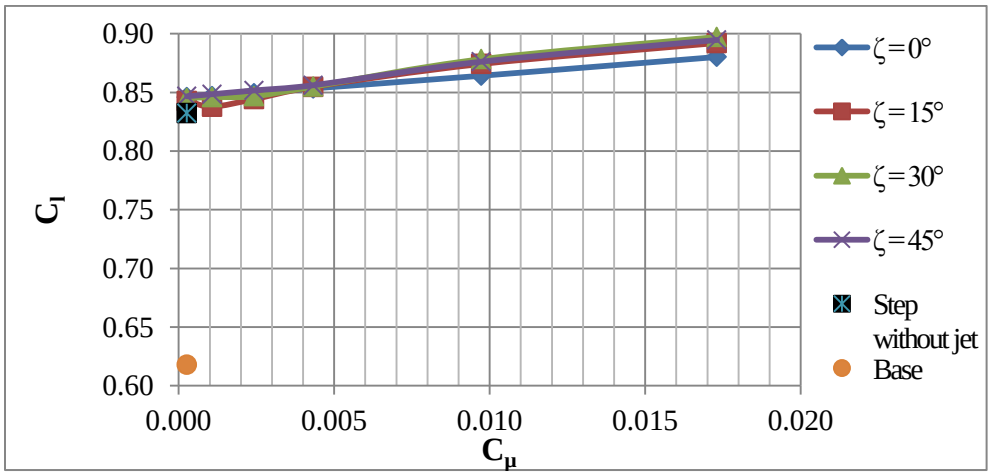

(a).

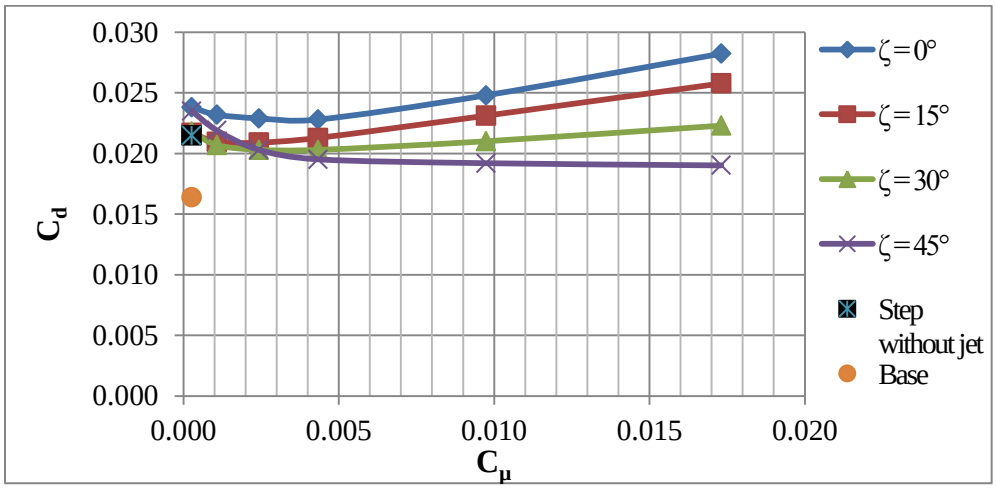

(b).

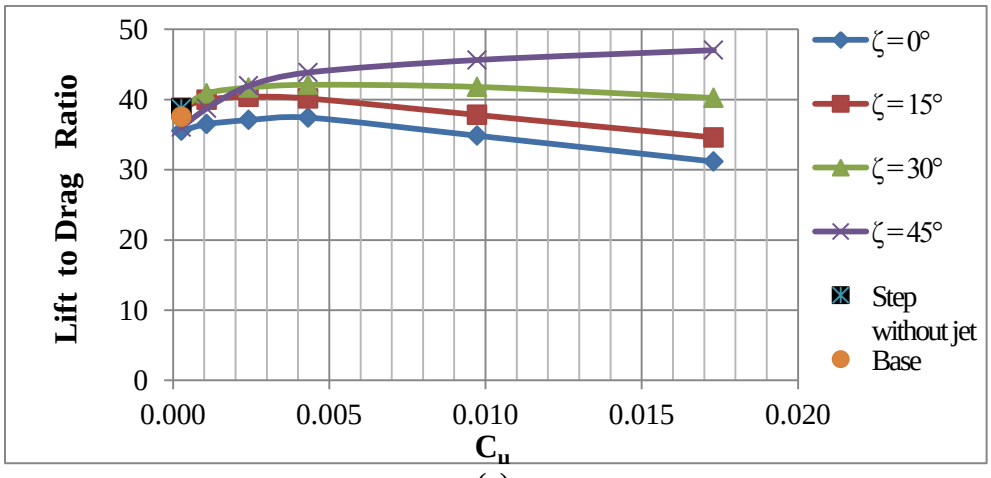

(c).

Figure 3-26: Dependence of the aerodynamic characteristics on ζ and Cμ when compared with the NACA 4415 airfoil cases without jet at α = 2°; Re = 1.7 million. (a) Lift; (b) Drag; (c) Lift to Drag Ratio

aerodynamic characteristics. The values of lift coefficient for all the jet cases are higher than that of the case without jet. Though there is a variation in C_l as the jet angle is varied while also varying the jet velocity from $0.25U_\infty$ to U_∞ thereby increasing $C\mu$ from 0.00027 to 0.00108, its dependence on jet angle varied from 15° to 45° seems to be diminishing as the jet velocity is increased beyond the magnitude of U_∞. As can be seen in the figure, C_l for the case of step without jet is 0.8324. With the activation of the jet at $\zeta = 0°$, and $C\mu = 0.00027$ corresponding to $V_j = 0.25U_\infty$, the C_l increases to 0.8460. As the jet velocity is increased to its peak value of $V_j = 2U_\infty$, with $C\mu = 0.01731$ at $\zeta = 0°$, there is a further rise in C_l to 0.8802 which is about 6% higher than the value for the step without jet case. There is a steady increase in C_l as the jet velocity is increased keeping ζ fixed at 0°. For the case of jet at $\zeta = 15°$, the C_l obtained is 0.8427 which is lesser than the value for the case of step without jet. There is a slight drop in C_l as the jet velocity is increased from $V_j = 0.25U_\infty$ to $0.5U_\infty$ correspondingly $C\mu$ from 0.00027 to 0.00108. This observation could possibly be understood from the Figure 3-23 which shows the velocity contours and streamlines colored by dimensionless velocity in the region of step cavity. The jet injected at an angle of 15° hits the outer layers of the large primary vortex. The jet injected at this particular jet velocity of 12.465 m/s seems to be ineffective in controlling the trapped vortex which is supported by the pressure contour plots shown in Figure 3-23. As can be noticed from the plots, there is only a slight variation in the pressure when compared with the pressure plots for the cases of step without jet and the jet cases shown by Figure 3-24. By comparison, the C_l obtained for another jet case for the same angle by increasing the jet velocity Vj from $0.5U_\infty$ to $0.75U_\infty$ with $C\mu = 0.00243$ is 0.8443 which is higher than that of the value for the case of step without jet. Also, the C_l increases consistently with increase in the jet velocity till it takes its maximum value of 0.8921 at $C\mu = 0.01731$ corresponding to the peak jet velocity $V_j = 2U_\infty$ as shown by the corresponding plot in Figure 3-26(a). When the jet angle is set at 30°, the C_l obtained is 0.8451 at $V_j = 0.25U_\infty$. With increase in the jet velocity there is a gradual rise in C_l

until the jet velocity takes the value of U_∞; the corresponding Cμ increased from 0.00027 to 0.00433. As V_j is increased further beyond U_∞ till $V_j = 2U_\infty$; Cμ = 0.0173, there is a rapid increase in C_l consistent with the increment in the jet velocity. Increasing the jet angle to 45° produces more interesting results. The jet parameters $\zeta = 45°$; $V_j = 0.25U_\infty$; Cμ = 0.00027 give a C_l of 0.8467, the highest for any jet case studied here at the lowest jet velocity. The C_l plot for the case of jet angle fixed at 45° follows the same trend as that of the case of $\zeta = 30°$ as the jet velocity is increased from $0.25U_\infty$ to U_∞; Cμ from 0.00027 to 0.00433 and increased till V_j equals $2U_\infty$ and Cμ = 0.0173. But beyond U_∞ the values of C_l are higher for the jet case at $\zeta = 30°$. The best results overall are obtained for the jet cases of jet angle equal to 30° and 45°. The case with jet angle $\zeta =$ 30° produces the highest C_l about 8% higher than the value for the stepped airfoil case without the use of jet at the maximum value of Cμ equal to 0.01731 corresponding to a jet velocity $V_j =$ $2U_\infty$ for the case of $\alpha = 2°$, and Re = 1.7 million which is evident from the C_p plot shown in Figure 3-25(e). The maximum pressure occurring on the airfoil surface downstream of the step face is higher in case of the jet case for $\zeta = 30°$ than that for $\zeta = 45°$. Figure 3-26(b) shows the drag data. It can be observed from the plots that the drag for some jet cases is lesser than that of the case without jet, the trend is opposite for some other jet cases, while for the rest of the cases, there is a slight or no variation as compared to value for the case of step without jet. The least C_d is obtained for the case with $\zeta = 45°$ at Cμ = 0.01731. For the all cases studied but one with $\zeta =$ 45°, the C_d curve shows a decreasing trend which is quite interesting. In the cases associated with jet used in this study, the concept of jet flap could possibly be used to understand the reduction in drag in the jet case for $\zeta = 45°$. A component of the jet momentum acts in the direction opposite to the free stream thus canceling a part of the drag resulting from the introduction of the step. According to Richard L.Kline as described in his 1985 article titled *The Ultimate Paper Airplane*[2], a stepped airfoil traps some of the displaced air molecules, reverses their direction, and produces a forward "push" which he called the "drag utilization". In other words, a force in the

direction opposite to drag is created due to the flow field developments or the vortex systems energized by the action of jet placed within the step cavity due to which there is an identifiable reduction in the drag which is supported by the results shown in Figure 3-26(b). Use of jet with $\zeta = 45°$ at $C\mu = 0.01731$ to control the flow field in the step cavity appears to be working the best following this concept of "drag utilization" and the result is, optimum aerodynamic characteristics, in this case the consistent decrease in C_d.

These changes in the lift and drag resulting from the use of jet might affect pitcihng moment considerably. Further investigation is required to rule out the possibility of having to expend usable power to obtain the benefits in aerodynamic performance to control the resulting changes in the pitching moment when the jet is used in the step cavity which might nullify the benefits produced by the jet. Figure 3-26(c) shows the plots showing the variation in the lift to drag ratio as the jet parameters are varied. The lift to drag ratio is the highest for the jet case with ζ equal to 45° at the highest value of $C\mu$. Thus the jet case with $\zeta = 45°$ and $C\mu = 0.01731$ produces the best results in terms of the aerodynamic performance quantified by the L/D ratio of the modified NACA 4415 airfoil case with jet which is about 21% higher than that of the case for step without jet as illustrated in the figure.

3.2. EXPERIMENTAL RESULTS

This section deals with the results and discussion of the experimental data obtained through the wind tunnel testing of a NACA 4415 airfoil based wing-model. The experimental part of the present research comprises of the measurements of forces. Force measurements were made to calculate the aerodynamic forces and the corresponding coefficients about the test model built with a panel for varying the step depth on the lower step configuration during the testing. Forces were measured over a stepped wing test model for a step length of $L_l = 0.5$, $D_l = 0.0$ (base airfoil), $D_l = 0.1, 0.2, 0.3, 0.4$ & 0.5 (stepped airfoil configurations). Due to the limitation of the

maximum airspeed that could be achieved in the tunnel, force measurements were feasible only for Re as high as 0.6 million. Efforts were made to record some useful flow visualization data using the in-house LED based lighting system. However, due to the unavailability of a sophisticated flow visualization system, quality images revealing the flow field developments including vortical structures, reattachment information for the various tested configurations could not be captured. Figure 2-6 shows a sample image capturing the flow over the wing model with step fully deployed during the wind tunnel testing.

Aerodynamic forces acting on the NACA 4415 based wing model were recorded during the wind tunnel testing using force balances. The lift and drag data obtained were processed to compute the aerodynamic coefficients, C_l and C_d. The values of lift to drag ratio were then computed using the C_l and C_d values. Figure 3-27 presents the plots illustrating the variation of C_l, C_d, and the lift to drag ratio for the cases of base airfoil (the case with $D_l = 0.0$) and the modified airfoil configurations studied (cases formed by varying the step depth from $D_l = 0.1$ to 0.5). Lift coefficient plots presented in Figure 3-27(a) show that the lift increases slightly as the step depth is increased from $D_l = 0.1$ to 0.5. The C_l values obtained are the highest for the case with $D_l = 0.5$ amongst all the cases studied. Drag coefficient plots presented in Figure 3-27(b) show that the trend is exactly the same as that observed in the C_l plots. The drag increases as the step depth is increased. The base airfoil case produces the least drag while the stepped airfoil case with $D_l = 0.5$ produces the highest. The results shown in this figure follow the same trend as that observed in the numerical results. As can be seen from the Figure's 3-27(a) and (b), the experimental values of drag obtained in proportion with the lift are significantly high as compared with the numerical lift and drag values for a given step configuration. Hence the experimental values of lift to drag ratio obtained are lower than the numerical values. Figure 3-27(c) shows various plots illustrating the variation in the value of the lift to drag ratio with change in the angle of attack. While analyzing in qualitative terms, it can be noted that the lift to drag ratios decrease

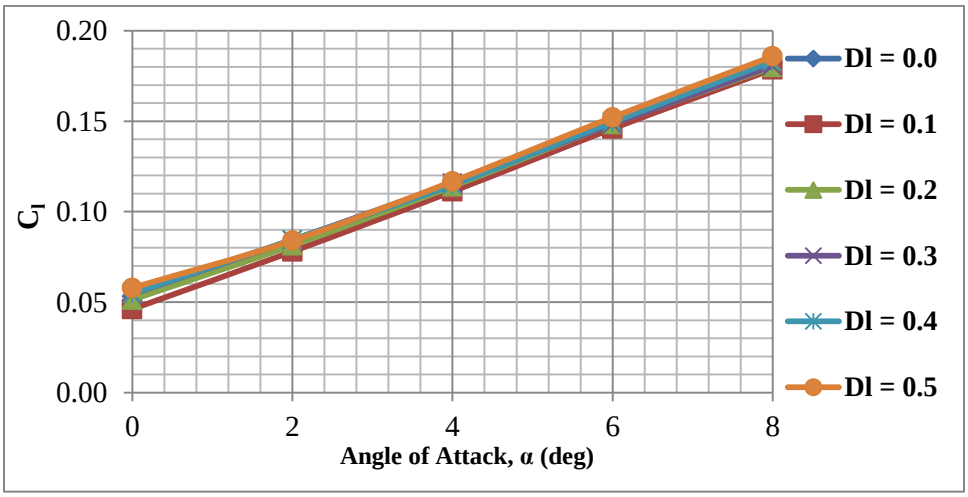

(a).

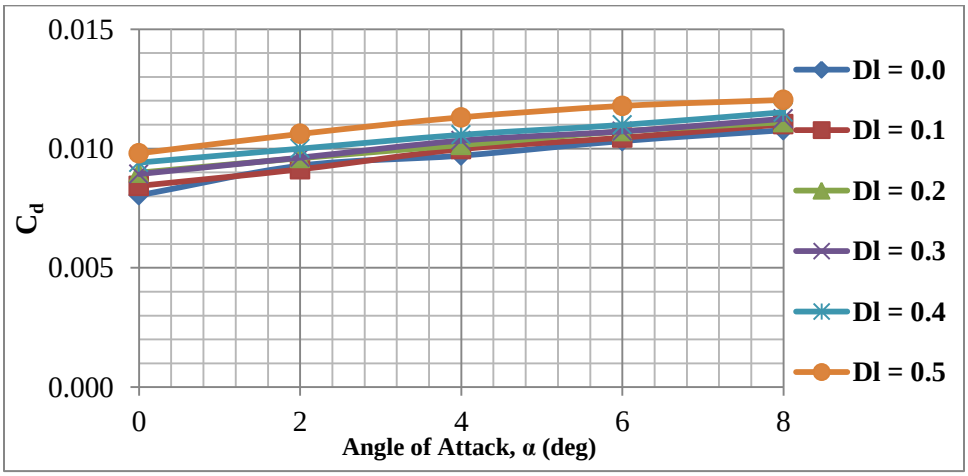

(b).

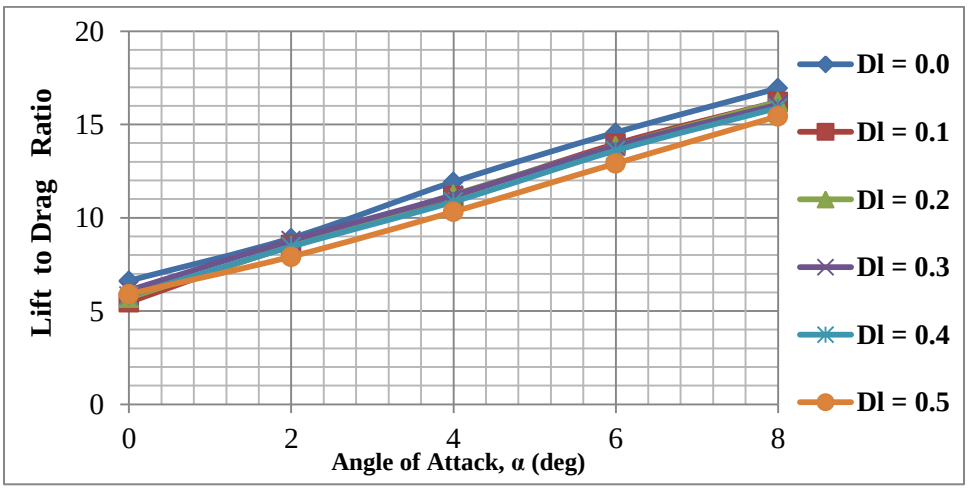

(c).

Figure 3-27: Variation of aerodynamic characteristics with angle of attack at Re = 0.6 million. (a). Lift; (b). Drag; and (c).Lift to Drag ratio

with increase in the step depth for the stepped airfoil configurations.

One of the cases of particular interest is the airfoil configuration set at $\alpha = 4°$, Re = 0.6 million. This particular case was tested to serve the purpose of validating the numerical results (presented in Figures 3-13 and 3-14) obtained for the same set of aerodynamic parameters and inlet conditions. Comparing the experimental and computational results , it is apparent that at Re = 0.6 million, the base airfoil produces better aerodynamic characteristics, i.e. higher lift and lower drag thus resulting in higher lift to drag ratios than those obtained with the stepped airfoil configuration. Thus the experimental result validates the one and only numerical case among all the cases studied for which the introduction of step on the lower surface seems to be ineffective in delivering better aerodynamic performance than the base airfoil case. The consistency noticed in the lift to drag ratio results from the increase in lift coefficient due to the introduction of step on the lower surface at about the entire range of attack tested just as predicted by the computational results obtained for the base airfoil and stepped airfoil configurations. Referring to the Figures 3-3(a) and 3-7(a), it can be concluded that for the case with Re = 0.6 million for the stepped airfoil configuration set at $\alpha = 4°$, the vortex formed in the step cavity is not strong enough to alter the flow field characteristics so as to enhance the aerodynamic performance. The influence of step and jet on the pitching moments however needs to be investigated.

4. CASE STUDY

This research effort explored the possibility of using a combination of passive and active control techniques to investigate the aerodynamic performance of conventional NACA 4415 airfoil using steps. The case study discussed here was aimed at the application of usable results obtained from the research conducted to a reconnaissance plane on a strategic mission considering various stages of flight to define our problem. The flight regimes include take-off & climb, cruise/reconnaissance, descent & landing, before the mission is completed. The current study focused on pointing out the benefits with regard to the aerodynamic performance, arising from a stepped airfoil replacing a conventional airfoil on a real life Unmanned Aerial Vehicle (UAV). The aircraft of interest was the RQ-2 Pioneer which was operational with the Navy, Marine Corps, and Army since 1986. Pioneer uses a NACA 4415 airfoil. This tactical reconnaissance and surveillance UAV operates in a Reynolds number ranging from 1.8 million to 3 million. Figure 4-1 shows the drawings of RQ-2 Pioneer. All the major technical specifications[10] are shown in Table 4-1. Figure 4-2 shows an operational RQ-2 Pioneer in flight.

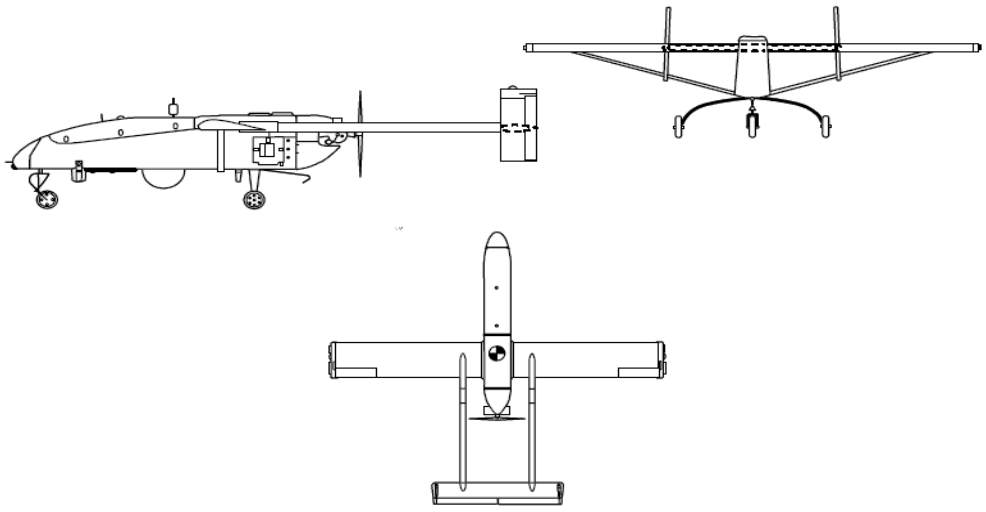

Figure 4-1: Schematic drawings[18] of RQ-2 Pioneer (RQ stands for Reconnaissance).

Table 4-1: Technical Specifications of the UAV RQ-2 Pioneer.

Length	4.27 m (14 ft 0 in)
Wingspan	5.15 m (16 ft 10.75 in)
Height	1.00 m (3 ft 3.5 in)
Weight	max: 205 kg (450 lb); empty: 178 kg (392 lb)
Speed	max: 204 km/h (127 mph); cruise: 120 km/h (74 mph)
Ceiling	4570 m (15000 ft)
Range	185 km (100 nm)
Endurance	5 hours
Propulsion	Sachs & Fichtel SF2-350 piston engine; 19.4 kW (26 hp)

Figure 4-2: RQ-2 Pioneer in flight. Courtesy: http://www.military.com/

The phases of flight envelope studied as a part of this research effort were limited to take-off, climb, and cruise which corresponds to the reconnaissance mode, assuming that the descent and landing modes of flight are similar to climb and take-off with regard to the flight conditions. Amongst the flight phases, take-off and climb are the shortest, cruise being the longest and the most crucial phase for a reconnaissance plane. Since endurance is directly affected by the lift to drag ratio, it is an important performance parameter for any a reconnaissance plane and any reduction in drag achievable with complementary increase in lift can considerably enhance the aerodynamic performance of the plane. Otherwise any combination of lift and drag resulting in a lift to drag ratio higher than that obtained with a conventional NACA airfoil is beneficial which brings the application of passive and active flow control techniques into the current picture.

The best stepped configuration was identified for each flight mode on the envelope. The data was mapped for the mission-specific objectives of a reconnaissance mission. Figures 3-9 through 3-14 illustrate the summary of the various cases studied from which useful results were picked for this case study. The flight regimes associated with the various cases are discussed in the next section. Results for the three phases of the entire flight envelope viz., the take-off, climb and cruise are discussed in the following sections.

4.1. WORKING ASSUMPTIONS

The chord of the NACA 4415 airfoil is 1 meter. All the experimental airfoil data available are for airfoils of unit chord length. For uniformity and ease of comparison of results obtained, the NACA 4415 airfoil with its actual chord of length 0.77 m as used on the UAV Pioneer was scaled to 1 m. The climb velocity of the UAV RQ-2 Pioneer studied here was assumed to be about 1500 ft. per min. The stall velocity was assumed to be around 95 km/h. The lift-off velocity was presumed to be equal to 1.3 times the stall velocity. The angles of attack

during the take-off, climb, and cruise were assumed to be 4°, 8° and 2° respectively. Based on the technical specifications available for the UAV, the wing loading was computed to be 502 N/m^2.

4.2. RESULTS AND DISCUSSION

4.2.1. Application of Passive Flow Control. This section discusses the application of the results obtained from studying the modified airfoil cases for a range of angles of attack and Reynolds number's. Corresponding to the flight conditions for each phase of flight, the results were picked for specific values of α and Re. The case study presented below discusses the Take-off; Climb; and the Cruise phases of flight of the UAV RQ-2 Pioneer.

4.2.1.1. Take-off phase. Numerical simulations were conducted using a conventional NACA 4415 airfoil considered as the base airfoil and the modified airfoil as an airfoil with an intermediate step on the lower surface. Results obtained show that lift coefficients are higher for the stepped airfoil than the base airfoil and the magnitude of the change in C_l increased with increase in the angle of attack. On the other hand, the drag values are higher for the stepped airfoil. Based on the C_l and C_d values obtained for each of the cases, the take-off distance is calculated using the following formula:

$$S_{TO} = (1.44\, W_0^2) / [g\, \rho_\infty\, S\, C_{lmax} (T- (D + \mu_r (W_0-L))] \quad (4.1)$$

The thrust T was estimated from the rated power of the UAV per the technical specifications listed in the Table 4-1 and the average velocity during the take-off which was obtained by averaging the velocities corresponding to the Re's of 0.6, 1.2, and 1.8 million occurring during the take-off phase. Also, the lift L and the drag D were computed using the average velocity occurring during the take-off phase. The minimum take-off distance for the base

airfoil case is about 155m while for the stepped airfoil case it is about 127m. Hence the ratio of S_{TO} for the stepped airfoil to the S_{TO} for the base airfoil equals 0.82 which means the use of an intermediate step defined by Xs=0.5, Ls=0.5, Ds=0.5 yields an 18% reduction in the minimum take-off distance required as supported by the computational results discussed in the previous section. This reduction mainly results from the increase in C_l due to the step. With the rise in C_l there is an increase in the lift. Also, the L/D ratio computed from the lift and drag data for the stepped airfoil case is higher than that for the base airfoil case.

Some simulations were run for cases at two intermediate Reynolds numbers lower than the value for lift-off. The two Reynolds numbers chosen are 0.6 and 1.2 million, while the maximum take-off Re is 1.8 million. Figure(s) 3-13 and 3-14 illustrate the ΔC_l and L/D ratio plots for all the take-off cases. At the peak Re which is 1.8 million, the C_l values just like the L/D ratios for the stepped airfoil are higher than those for the base airfoil as shown in the figures. The trend is the same for the Re 1.2 million. When the Re is 0.6 million, the results obtained do not follow the same trend as that of the other cases, though the C_l values are still higher than those for the base case at the same Re number. The L/D ratios for stepped airfoil cases are less than those for the base airfoil because of relatively higher drag.

4.2.1.2. Climb phase. The conditions for the fastest climb/ maximum climb rate were assumed for the numerical investigation. The climb velocity at these conditions is 37.53 m/s. The corresponding Reynolds number is 2.5 million. The climb angle is 9˚. The angle of attack is 8˚. There is about 20% increase in the C_l over the base airfoil as illustrated in Figure(s) 3-15 and 3-16. Also the L/D ratio increases by 11%.

4.2.1.3. Cruise phase. The cruise Reynolds number is 1.7 million, the velocity being 24.93 m/s. The use of step yields about 34% higher C_l than the base airfoil and the L/D

ratio increases by 3%. Figure(s) 3-11 and 3-12 show the ΔC_l and L/D ratio plots for the cruise case corresponding to $\alpha = 2°$. This increase in the L/D ratio yields about 20% increase in the endurance (E) of the UAV RQ-2 Pioneer with the use of stepped airfoil over the conventional NACA 4415 airfoil. The endurance of the UAV with a conventional NACA 4415 airfoil based wing is 5 hours. The ratio $E_{\text{stepped airfoil}} / E_{\text{base airfoil}}$ was computed to be 1.2 meaning the endurance could be increased to about 6 hours or a 20% increase in the endurance could be obtained by employing the step on the lower surface. The endurance and range calculations were made using the equation's below:

$$E = (\eta/c_s)*(C_L^{3/2}/C_D)*(2\rho_\infty S)^{1/2}*(W_1^{-1/2} - W_0^{-1/2}) \quad (4.2)$$

$$R = (\eta/c_s)*(C_L/C_D)*\ln(W_0/W_1) \quad (4.3)$$

η was assumed to be 0.8 for all the calculations while c_s was assumed to be 2.27e-7 ft^{-1}. Range was computed for both the base and stepped airfoil configurations. The ratio $R_{\text{stepped airfoil}} / R_{\text{base airfoil}}$ was calculated to be around 1.03 which means the activation of lower surface step during the cruise results in an increase of about 3% over the conventional NACA 4415 airfoil based wing originally used on the UAV Pioneer.

4.2.2. Step Schedule. The step is activated as the airspeed approaches the value corresponding to a Re of 0.6 million during the take-off. Results obtained from simulations at higher Re occurring during climb and cruise phases of flight show that the step defined by Xs=0.5, Ls=0.5, Ds=0.5 produces better aerodynamic characteristics than the conventional NACA 4415 airfoil. Thus the step could be held activated during the flight regimes of climb and cruise. Similarly, it could be held activated during the descent and landing. Complementing the rise in C_L and correspondingly the L/D ratios, there will be increase in the pitching moments which will also affect the performance of the airfoil configurations. The current study did not

focus on the effect of variation of the pitching moments which needs to be investigated.

4.2.3. Application of Passive and Active Flow Control. The effect of using an air injecting jet into the step cavity was studied on a conventional flat faced step on the lower surface of a NACA 4415 airfoil. Figure 3-17(b) shows the location of the jet placed on the bottom of the step for all the jet cases discussed in this study. Since cruise is the longest and the prime operational phase of reconnaissance planes, this study focuses on the cruise phase. Active flow control using jet was employed on the modified NACA 4415 airfoil configuration to enhance the aerodynamic performance of the stepped airfoil in the cruise regime. Any benefits yielded by the jet would also be applicable to other flight regimes based on the results discussed earlier in this case study. Table 3-2 enlists all the jet cases studied along with the associated jet parameters ζ , and $C\mu$. Figure 3-25 shows the plots illustrating the aerodynamic characteristics of C_l, C_d, and L/D ratio for the various jet cases studied comparing them with the case of stepped airfoil without jet. The jet case for $\zeta = 45°$, and $C\mu = 0.01731$ produces the best results with regard to the aerodynamic performance. This case gives about 7.5% increase in C_l over the corresponding case without jet. Further, there is about 12% reduction in C_d. As a result, this jet case yields about 22% increase in the L/D ratio over its stepped counterpart without jet. To emphasize on the fact that the jet proves to be enhancing the aerodynamic performance, the results obtained here are enhancements over the stepped airfoil without jet which itself delivers enhancement of the L/D ratio over the conventional NACA 4415 airfoil. Getting back to the performance calculations, the endurance increases by about 26% due to the rise in the L/D ratio resulting from the employment of jet in the step cavity over the stepped airfoil case without jet. Employment of jet in conjunction with step on the lower surface of a NACA 4415 airfoil used on the UAV RQ-2 Pioneer could possibly result in as much as 50% increase in the endurance over the case of the aircraft using the conventional NACA 4415 airfoil. With the use of jet, the range increases by about 5% over the

stepped airfoil case without jet. This is a tremendous benefit to the aircraft in terms of the efficiency and could result in a huge money savings and considerable reduction in emissions.

5. CONCLUSIONS AND OUTLOOK

The results presented in this thesis constitute the next step towards understanding the effects of a step-induced vortex on the aerodynamic characteristics of a conventional NACA 4415 airfoil for a range of Reynolds number's and angles of attack. This study takes on a relatively new family of airfoils which are yet to be researched extensively. The objective of the study was to enhance the aerodynamic performance of the stepped NACA 4415 airfoil for a chosen range of Reynolds numbers and angles of attack, following on the preliminary studies conducted on stepped airfoils in the past by other researchers from around the world. The airfoil with a backward facing step on the lower surface was shown to have the potential to enhance the aerodynamic characteristics by increasing the lift coefficients and lift-to-drag ratios considerably in most cases and substantially in some of the cases studied through this research. Use of jets was proved to be effective in enhancing the aerodynamic performance of stepped airfoils.

Based on the results obtained by Stephen Witherspoon[7] and Fathi Finaish (1996), the airfoil configuration with a step on the lower edge step located at mid-chord, with a step depth half of the mid-chord airfoil thickness and extending till the trailing edge was chosen as the common configuration for all the cases studied in this research effort. Special focus was placed on enhancing the aerodynamic performance of this stepped airfoil configuration with the application of active flow control using air injecting jet placed in the step cavity.

Results obtained show that the lift coefficients were higher by as much as 37% for the best case among all the stepped airfoil cases studies in the range of α's i.e. $\alpha = 2°$, 4°, and 8° and the entire range of Reynolds number's i.e. Re = 0.6 million to 2.5 million. The application of active flow control proves to be effective in enhancing the lift of the stepped airfoils studied at Re = 1.7 million; $\alpha = 2°$. The lift coefficients were higher for all the jet cases, significantly high in

many jet cases and slightly high in some based on the setting of the jet parameters ζ, the jet angle and V_j, the jet velocity. The stepped airfoil case using jet with ζ = 45° and Cμ = 0.01731 corresponding to $V_j = 2U_\infty$ produces the best results in terms of the aerodynamic performance enumerated by the values of L/D ratio of the modified NACA 4415 airfoil case with jet which are significantly higher than that obtained for the case of step without jet and other jet cases, though the maximum C_l occurs at Cμ = 0.01731 for ζ = 30°. The contribution to the highest L/D ratio obtained in the jet case for ζ = 45° comes from the reduction in C_d which is significanlty higher than in the jet case for ζ = 30° at the same Cμ as compared with the C_d obtained in the case of step without jet.

Drag-coefficient data indicate that with the introduction of a step, drag increased. This observation is consistent in all the modified airfoil cases studied. The use of active flow control in the form of an air injecting jet in the step cavity of the modified airfoil configuration produces some promising results for the jet cases studied at Re = 1.7 million; α = 2°, with higher benefits in terms of drag reduction over the stepped airfoil cases when compared with the drag data for the base airfoil cases. For jet cases formed by the combination of various ζ's of 0°, 15°, 30°, and 45°; Cμ's of 0.00027, 0.00108, 0.00243, 0.00433, 0.00974, and 0.01731 corresponding to $V_j = 0.25U_\infty$, $0.5U_\infty$, $0.75U_\infty$, U_∞, $1.5U_\infty$, and $2U_\infty$ respectively, the drag data obtained are either less than those of the case of step without jet or show little variation from those values. However, there is a reduction in drag by about 12% over the stepped airfoil in the step with jet case with jet parameters ζ = 45° and Cμ = 0.01731 which is the case of interest in this study.

The lift-to-drag ratios were higher for all the stepped airfoil cases studied except for the case of Re = 0.6 million at α = 4°, proving once again that a stepped airfoil is superior to a conventional NACA airfoil with regard to the aerodynamic performance. The lift to drag ratio is maximum for the case of Re = 2.5 million at α = 4°. Higher lift-to-drag ratios are obtained using

jet in the step cavity for some of the cases studied at Re = 1.7 million; $\alpha = 2°$. For the jet case with $\zeta = 30°$, as the jet velocity is increased, the values obtained show little variation from that of the stepped airfoil case without jet. For the jet cases with $\zeta = 0°$ and 15°, the lift-to-drag ratios obtained by varying the jet velocity are lesser than the value for the case of step without jet in most of the cases studied. The case of interest is the jet set at 45° in which case the lift-to-drag ratios are considerably higher for most cases studied by varying the jet velocity. The best results are obtained for the case of $\zeta = 45°$ and $C\mu = 0.01731$ which produces an L/D ratio which is about 22% higher over the stepped airfoil case without jet that gives a value about 3% higher than the NACA 4415 considered as the base airfoil for all the cases studied in this research. As discussed earlier, the influence of the jet on the pitching moments due to the changes in the lift and drag needs to be investigated.

Flow control is one of the most promising and the most sought after areas of research in the field of fluid mechanics and aerodynamics. Achieving an enhancement in the aerodynamic performance correlates to improving the overall efficiency of the aircraft as a significant amount of power could be saved due to the reduction in drag and / or increase in the lift resulting in huge fuel and money savings and most importantly reduced emissions. Future work in the direction of the current research with the application of flow control and the preliminary studies conducted on stepped airfoils in the past could possibly involve experimental investigation of a full-scale model of RQ-2 Pioneer using the modified NACA 4415 airfoil based wing; and further numerical and experimental investigation towards the design, development and testing of feedback control based devices aimed at enhancing the aerodynamic performance of the modified airfoils with steps operational on the entire flight envelope designed for a particular mission.

REFERENCES

[1] NACA Report No. 460, "The Characteristics of 78 Related Airfoil Sections from Tests in the Variable-Density Wind Tunnel", (summary of airfoil data), 1935. http://ntrs.nasa.gov/archive/nasa/casi.ntrs.nasa.gov/19930091108_1993091108.pdf

[2] Kline, Richard, "The Ultimate Paper Airplane", Simon and Schuster, New York, NY, 1985.

[3] Fertis, Demeter G., "New Airfoil Design Concept with Improved Aerodynamic Characteristics", Journal of Aerospace Engineering, Vol. 7, NO. 3, pp. 328-339, July, 1994.

[4] Gad-el-Hak, M, "Control of low-speed airfoil aerodynamics", AIM J., 28(9), 1537-1552, 1990.

[5] Witherspoon, S., and Finaish, F., "Aerodynamic Characteristics of Airfoils with Backward-Facing Step Configurations", SAE Paper No. 961297, Proceedings, SAE Aerospace Atlantic Meeting, Society of Automotive Engineers, Warrendale, Pa., May 1996.

[6] Witherspoon, Stephen, and Finaish, Fathi, "Experimental and Computational studies of flow developments around an airfoil with backward-facing steps", American Institute of Aeronautics and Astronautics, AIAA-96-2481-CP, 1996.

[7] Witherspoon, Stephen, and Finaish, Fathi, "Aerodynamic performance of an airfoil with step-induced vortex for lift augmentation", Journal of Aerospace Engineering, January 1998.

[8] Ringleb F.O., "Separation control by trapped vortices", In: Boundary Layer and Flow Control", Ed. Lachmann G.V., Pergamon Press, Oxford, pp. 265–294, 1961.

[9] Kasper W.A. "Some Ideas of Vortex Lift", Society of Automotive Engineers, Inc., Warrendale, PA, Paper 750547, pp 12, no date.

[10] The Directory of U.S. Military Rockets and Missiles, Department of Defense, United States**,** December 2011. http://www.designation-systems.net/dusrm/app2/q-2.html

[11] Kruppa E.W., "A Wind Tunnel Investigation of the Kasper Vortex Concept", AIAA, Paper 77-310, pp. 10, 1977.

[12] Yeung W.W.H., "Lift Enhancement on Unconventional Airfoils", Jurnal Mekanikal, No. 22, 17-25, December 2006.

[13] Fabrizio De Gregorio and Giuseppe Fraioli, "Flow Control on a High Thickness Airfoil by a Trapped Vortex Cavity", 14th Int Symp on Applications of Laser Techniques to Fluid Mechanics, Lisbon, Portugal, July 2008.

[14] Huang.A, Folk.C, Ho.C.M., Liu.Z, Chu.W.W., Y. Xu, Tai.Y.C., "Gryphon M^3 System: Integration of MEMS for Flight Control", MEMS Components and Applications for Industry, Automobiles, Aerospace, and Communication, Conference Proceedings of SPIE Vol. 4559, 2001.

[15] Crittenden.T, Glezer.A, Birdsell.E, and Allen.M, "Microfabricated, Combustion-Driven Jet Actuators for Flow Control Applications", American Physical Society, 54th Annual Meeting of the Division of Fluid Dynamics, November 2001.

[16] Schadow, Klaus, and El-Fatatry, Ayman, "Military/Aerospace MEMS Applications – AVT Task Group 078", RTO AVT Symposium on Novel Vehicle Concepts and Emerging Vehicle Technologies, Brussels, Belgium, RTO-MP-104, April 2003.

[17] Boroomand Masoud and Hosseinverdi Shirzad, "Numerical Investigation of Turbulent Flow Around A Stepped Airfoil At High Reynolds Number", American Society of Mechanical Engineers (ASME) Fluids Engineering Division Summer Meeting, August 2009.

[18] Wikipedia, the free encyclopedia.

[19] Kohlman, David L., "Introduction to V/STOL Airplanes", Iowa State University Press / Ames, First Edition, 1981.

[20] *Independent Scientific Testing*, an excerpt from the article on KF airfoils, December 2008. http://en.wikipedia.org/wiki/Kline%E2%80%93Fogleman_airfoil#cite_note-0

[21] Kitsios.V, Kotapati.B.R, Mittal.R, Ooi.A, Soria.J, and You.D, "Numerical Simulation of Lift Enhancement on a NACA 0015 airfoil using ZNMF jets", Center for Turbulence Research, Proceedings of the Summer Program, 2006.

[22] Gad-el-Hak, M, "Modern developments in flow control", Applied Mechanics reviews Vol. 49, 365-379, 1996.

[23] Fabrizio De Gregorio, and Giuseppe Fraioli, "Flow Control on a high thickness airfoil by a trapped vortex cavity", 14th symposium on Applications of Laser Techniques to Fluid Mechanics, Lisbon, Portugal, July 2008.

[24] Linda D. Kral, "Active Flow Control Technology", ASME Fluids Engineering Division Technical Brief, April 2010.

VITA

Ranganadhan Voona was born in Berhampur, Orissa, India in the month of December, 1985. He is a citizen of India by birth. After finishing his Bachelor's degree in Aeronautical Engineering, he came to the U.S. to pursue his Master's degree in Aerospace Engineering at the Missouri University of Science and Technology, Rolla. In order to broaden his scope of interest for the jobs, he changed his Major to Mechanical Engineering given the many sensitivity issues associated with the jobs in the field of Aerospace.

His academic interests lie in the areas of applied aerodynamics, fluid mechanics, and structures. His specific interests are Flow Control, Wind Tunnel Testing, Aerodynamic Design and Analysis, Finite Element Analysis. After finishing his Master's program at Missouri University of Science and Technology, he has plans for gaining some work experience in the field of Aerospace / Mechanical Engineering. He was placed at Caterpillar and worked as a Component Application Engineer on the wheel loader machines during his Curricular Practical Training (CPT) program at Missouri S&T. His hobbies include Music and Singing, Photography, Writing, and Art to mention a few. He can be reached at vinayvoona@gmail.com for any subject discussions in Science, Technology or the amazing world of Aerospace!